FACULTY OF
MECHANICAL
ENGINEERING
CTU IN PRAGUE

Institute of design and machine parts

Design of a Robotic Manipulator for Loading of Strip Detector Staves

2022

Jan BRAJER

Study program:	(N2301) Mechanical engineering
Field of study:	(2301T047) Traffic, aircraft and transport technology
Supervisor:	Ing. Martin Janda

ZADÁNÍ DIPLOMOVÉ PRÁCE

I. OSOBNÍ A STUDIJNÍ ÚDAJE

Příjmení: **Brajer** Jméno: **Jan** Osobní číslo: **456773**

Fakulta/ústav: **Fakulta strojní**

Zadávající katedra/ústav: **Ústav konstruování a částí strojů**

Studijní program: **Dopravní a transportní technika**

Specializace: **Transportní technika**

II. ÚDAJE K DIPLOMOVÉ PRÁCI

Název diplomové práce:

Konstrukční návrh robotického manipulátoru pro zakládání modulů stripového detektoru

Název diplomové práce anglicky:

Design of a Robotic Manipulator for Loading of Strip Detector Staves

Pokyny pro vypracování:

Proveďte konstrukční návrh manipulátoru pro zakládání modulů stripového detektoru do jeho konstrukce. Manipulátor bude zakládat moduly do čtyř soustředných vrstev. Moduly budou v jednotlivých vrstvách naklopeny vzhledem k ose rotace detektoru. Manipulátor musí tedy umožnit rotační pohyb po kružnici v plném rozsahu, pohyb v radiálním směru pro změnu vrstev v rozsahu R=499mm až R=1000mm a naklopení modulu v rozsahu 0° až 13°. Potřebná délka pro zasunutí modulu je 1500mm. V rešeršní části práce se věnujte výběru vhodných typů pohonů, konstrukčních prvků a materiálů pro 3D tištěné díly. Dále proveďte rozměrovou analýzu konstrukce, MKP analýzu celku a optimalizaci kontrukce na základě poznatků získaných ze stavby prototypu a požadavků vzešlých z implementace řízení postaveného na základě průmyslového standardu.

Seznam doporučené literatury:

SHIGLEY, Joseph Edward, Charles R. MISCHKE a Richard G. BUDYNAS, VLK, Miloš, ed. Konstruování strojních součástí. Přeložil Martin HARTL. V Brně: VUTIUM, 2010. Překlady vysokoškolských učebnic. ISBN 978-80-214-2629-0.

Jméno a pracoviště vedoucí(ho) diplomové práce:

Ing. Martin Janda ústav konstruování a částí strojů FS

Jméno a pracoviště druhé(ho) vedoucí(ho) nebo konzultanta(ky) diplomové práce:

Datum zadání diplomové práce: **11.04.2022** Termín odevzdání diplomové práce: **08.08.2022**

Platnost zadání diplomové práce: _____

Ing. Martin Janda podpis vedoucí(ho) práce	Ing. František Lopot, Ph.D. podpis vedoucí(ho) ústavu/katedry	doc. Ing. Miroslav Španiel, CSc. podpis děkana(ky)

III. PŘEVZETÍ ZADÁNÍ

Diplomant bere na vědomí, že je povinen vypracovat diplomovou práci samostatně, bez cizí pomoci, s výjimkou poskytnutých konzultací. Seznam použité literatury, jiných pramenů a jmen konzultantů je třeba uvést v diplomové práci.

Datum převzetí zadání _____ Podpis studenta _____

DECLARATION

I declare that I developed the master thesis entitled: "Structural design of a robotic manipulator for the establishment of strip detector modules" independently under the supervision of Ing. Martin Janda using the sources listed at the end of my thesis in the list of used literature.

....

In Prague, day Jan Brajer

ACKNOWLEDGMENT

I would like to thank the supervisor of my thesis, Mr. Ing. Martin Janda, for valuable advice and all the help. I would also like to thank my colleagues at the Institute of Design and Machine Parts CTU, my family and my wife for their support.

NOMINATION SHEET

Name of the author:	Jan Brajer
Name:	Design of a Robotic Manipulator for Loading of Strip Detector Staves
Year:	2022
Study program:	(N2301) Mechanical engineering
Field of study:	(2301T047) Traffic, aircraft and transport technology
Institute:	Institute of designe and machine parts
Supervisor:	Ing. Martin Janda
Consultant:	Ing. Martin Janda
Bibliographic data:	
Number of pages	63
Number of figures	70
Number of tables	3
Number of attachments	7
Keywords:	Strip detector, Manipulator, Stave, Particle detector, 3D printing, Tilting, Aluminium profile

Abstract: In this work I design the manipulator to load the strip detector modules into its structure using 3D printing technology. The manipulator with virtual axis of rotation loads modules into four concentric layers. The modules are tilted in individual layers with respect to the axis of the detector rotation (need for the virtual axis of rotation). The manipulator must therefore allow rotational movement in a circle in the full range, movement in the radial direction to change the layers and tilting the module. Finding correct settings for 3D printing to achieve best results in terms of durability, toughness and mass reduction.

CONTENT

1 Introduction

The topic of this master thesis is the structural design of a robotic manipulator for the insertion of strip detector modules, which will meet the requirements set by the client (in this case CERN Atlas ITk) and respect all the boundary conditions given by the environment in which the manipulator will operate. Additionally a structural analysis of the stiffness of the device will be done, using the finite element method, which helps to evaluate the resulting stiffness of the device and its deformation during. The dimensional analysis will also be done in order to define the range of the settings required in order to align the device. In the next phase of the work, the selection and purchase of components and the completion of the prototype will take place in the laboratories of the Institute of Design and Machine Parts of the CTU and the subsequent validation of the equipment in the Rutherford Appleton Laboratory (referred to as RAL). At this time, the final step is to optimize the manipulator based on the information obtained during prototype testing and design and produce the updated version of the device.

1.1 Pixel detector

This chapter is focused on the pixel detector and how does it function, mainly the staves that will be inserted by the constructed device.

The pixel detector is the inner-most part of the inner detector of the ATLAS tracking system. It consists of 4 layers of barrel pixel detectors, which will be inserted by the tooling and two end caps of three pixel disks each. [1] The other parts, which the ATLAS tracking system consists of are the calorimeter, the muon chambers and the magnet, which together create the outer detector.

The main purpose of this detector is to track the trajectory of the charged particles, generated during the experiments in the Large Hadron Collider (referred to as the LHC). [2]

1.1.1 Staves

Staves are, as mentioned, the inner-most part of the detector and they consist of the pixels and strips, which then register the change of the magnetic field caused by the particle going through them. Based on this data, after the data processing the tracking of the particles is done.

Barrel and end-cap modules are supported by the carbon fibre cores. The core consists of the titanium pipes providing cooling, embeded in thermally conductive foam and carbon fibre honeycomb. The stave is designed to be cooled down to -35°C using the evaporative CO2 cooling system. Carbon fibre sheets, enclosing the

core from top and bottom, also carry a polymide tape on their outer face (figure 2), containing the power and transmission lines for the silicone modules (figure 3). Each stave also has an End-of Substructure card (EoS) which provides the connection with the rest of the structure. [3]

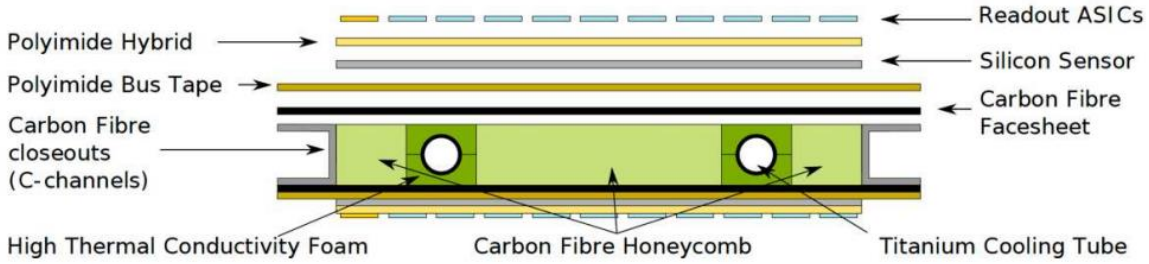

Fig. 1: Stave support structure [3]

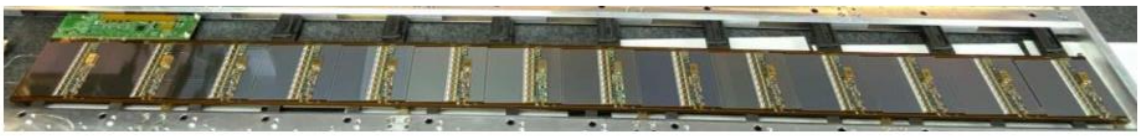

Fig. 2: Barrel stave with 14 strips [3]

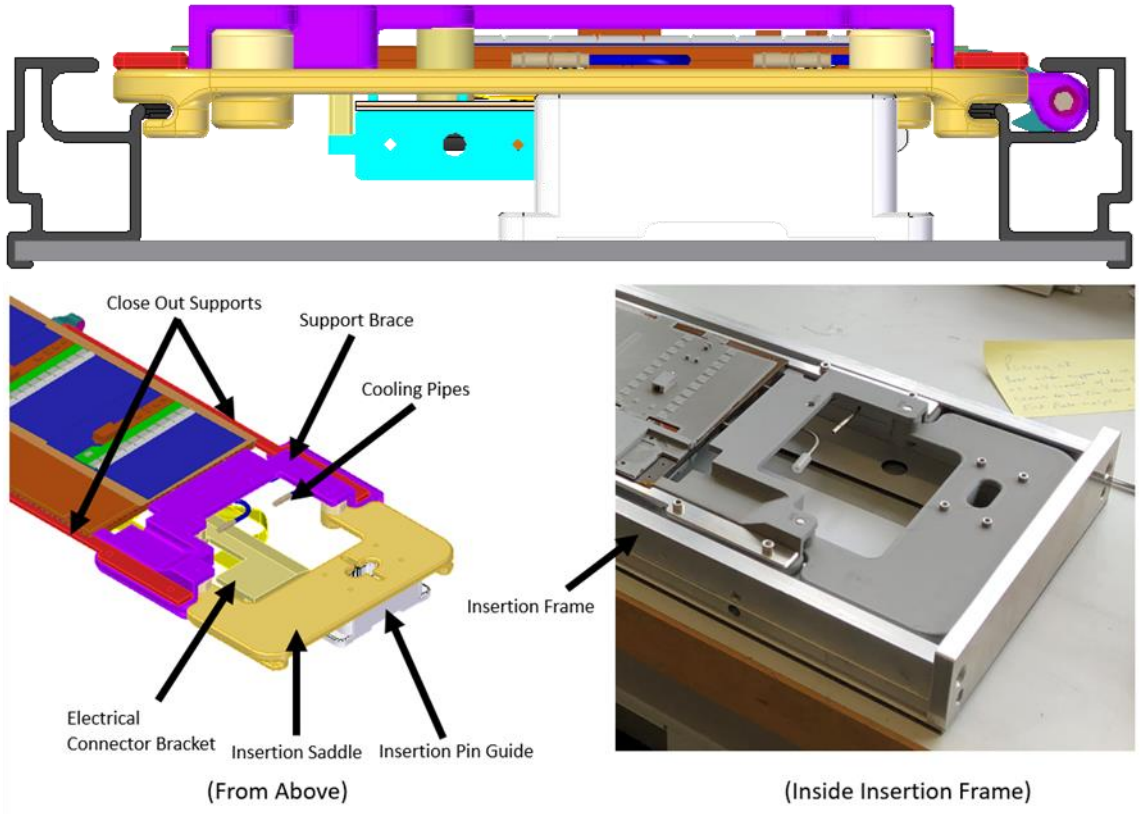

Fig.3: Strip in the box *[4]*

Staves are arranged in the circular pattern, in 4 layers (figure 4). In each layer, the strips are tilted to the plane tangent to the envelope by 11°/12°/13° and in total there is 196 staves for each side.

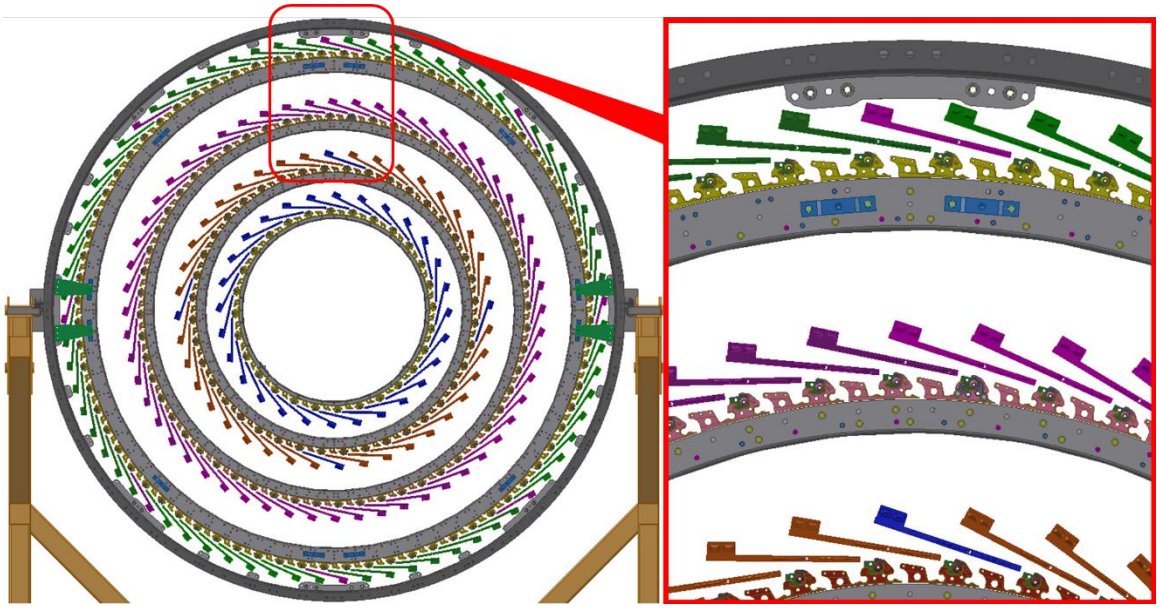

Fig.4: Tilt of the staves to the plane tangent to the envelope

Staves will be placed on top of the Stave insertion tooling (referred to as SIT) in the protective box (figure 3), so the SIT must be able to fully slide the stave out of the box.

1.2 Boundary conditions

The boundary conditions were defined mostly by the outer cylinder (figure 5), where the SIT will be positioned during its usage. The inner diameter of the outer cylinder is 2110 mm and the length is 1400 mm (figure 6). The SIT can continue out of the outer cylinder on its outer edge, but is must not exceed 1400 mm length within the outer cylinder (from the outer edge).

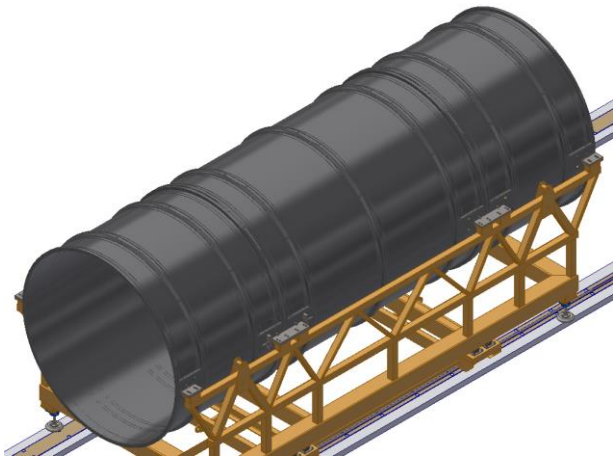

Fig.5: Outer cylinder

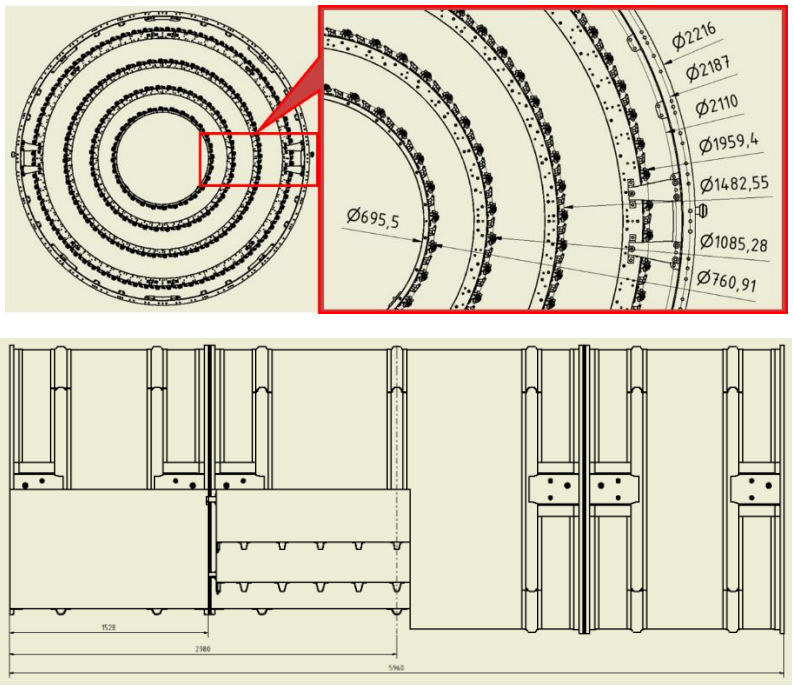

Fig.6: Limiting dimensions and the diameters of the layers

The outer cylinder constructions only offers 8 anchoring points, with spaced at 45° to anchor the SIT to, but only 6 of them are reserved for the SIT (figure 7). The wall of the outer cylinder is a thin composite structure and is fragile enough to be permanently damaged if the SIT colided with it, so the decision was made to prevent any contact of the SIT with the outer cylinder with a exception of the 6 anchoring points. The SIT must be thereby stiff enough to prevent any contact caused by the deformation (mostly bending) of the beams during the insertion process.

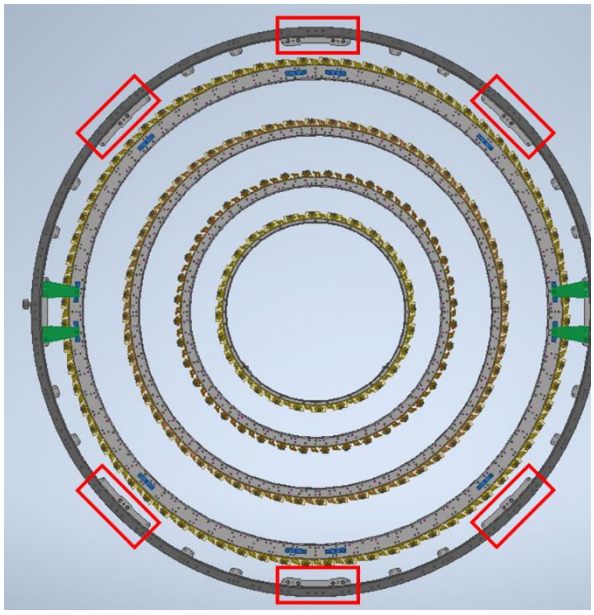

Fig.7: Anchoring points on the inner and outer edge of the outer cylinder

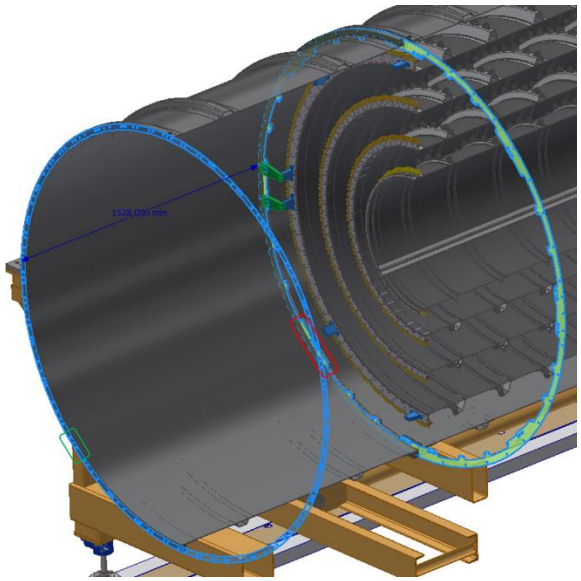

Fig.8: The distance between the outer (green) and inner (red) anchoring points

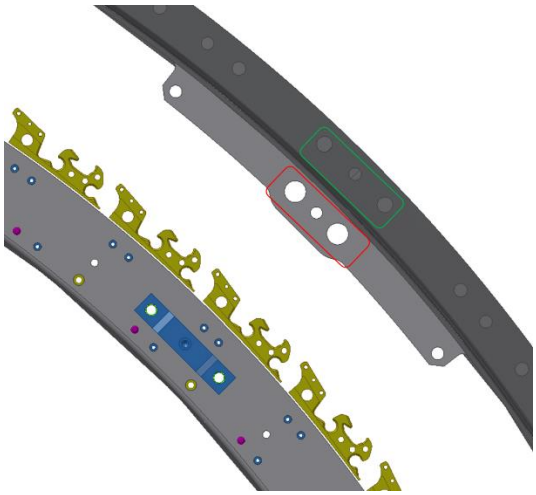

Fig.9: Anchoring point type 1 detail

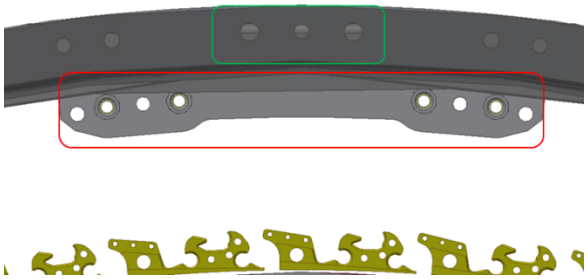

Fig.10: Anchoring point type 2 detail

Additionally the SIT must allow the removal of up to two legs without compromising the overall stiffness of the structure. So the construction must allow a quick and simple removal and mounting of any leg.

The movement requirements for the device are the rotation of the radial arm in full circle (the range can be 180° to both sides) and the extension of the carriage by 120 mm in the Z axis direction in order to overcome the gam for the services installation (Z indexing). The carriage itself must be able to tilt 0°/11°/12°/13°/14° to the radial arm and must be able to fully slide the stave from the box (1500 mm).

From the closer inspection of the placement of the stave inside the box and the brackets, that the stave is inserted into, is aparent that, the SIT carriage will have to be constructed with a virtual rotation axis in order to ease thepositioning process. The movements of the SIT are discussed in detail in the chapter 1.3.

Since the staves are very fragile, the SIT must achieve high stiffness and precision in order not to damage the staves during the insertion process, but the specific numbers were not yet specified. The device must also achieve a high repeatibility in order to guarantee the reliability and precision and to avoid any possible damage to the stave, SIT or its surroundings.

1.3 Movements done by the SIT

For the insertion of each module, the SIT must do 5 movements in a sequence. The following figures (11-13) describe the sequence of the movements of the SIT.

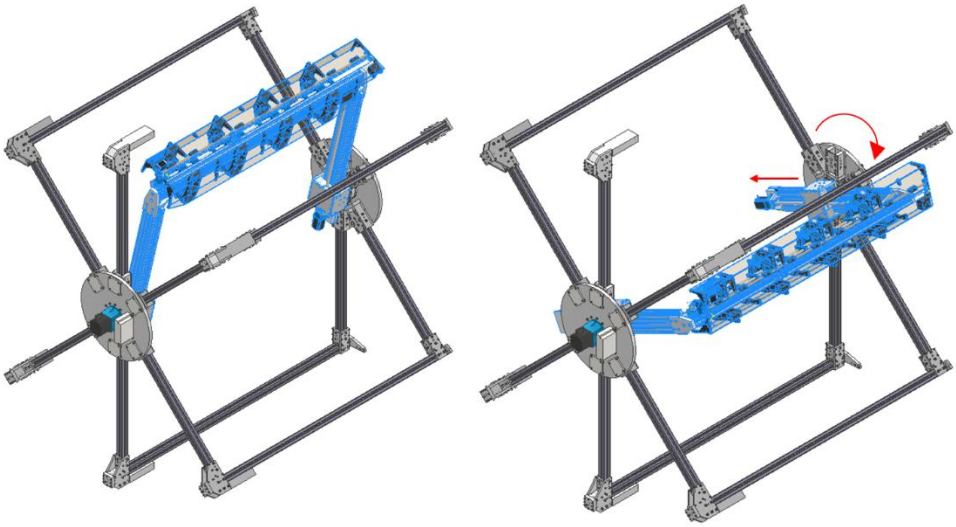

Fig.11: radial arm movement – rotation and the extension

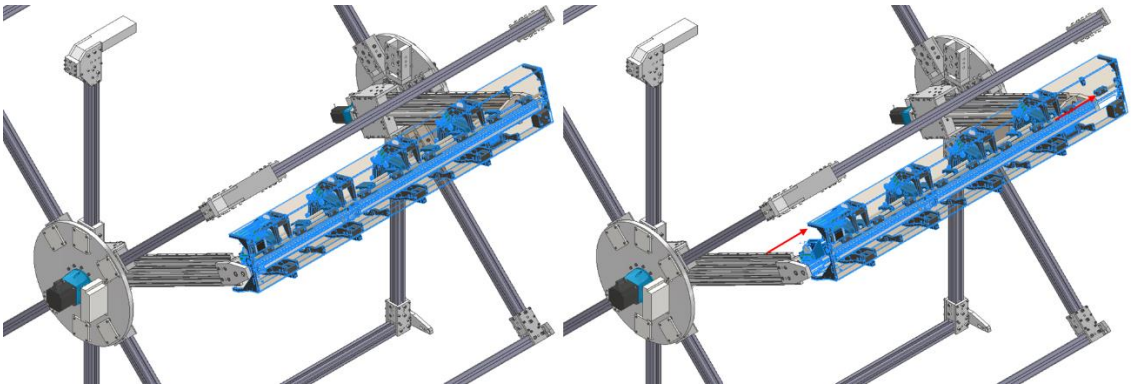

Fig.12: carriage movements – Z indexing and the stave sliding

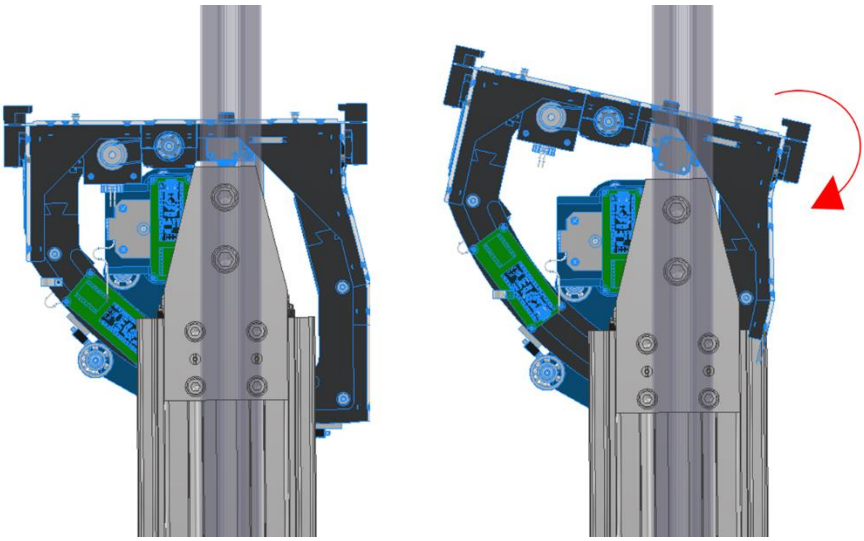

Fig.13: Tilting of the carriage

The sequence of the movements is following: First the SIT does the tilting of the carriage corresponding with the inserted layer and after that the SIT moves the carriage (by rotation and extension of the radial arm) to the “rough” position which is defined by the layer and the number of the stave. The “rough” position is achieved only via the steps done by the stepper motors and is not measured. The fine positioning is done using the camera in front of the carriage, which can by the visual control of the reference points achieve very high precision of the positioning and is able to calculate the steps needed for each stepper motor in order to align the axis of the stave with the axis of the corresponding bracket. The software controlling the SIT was not a part of my thesis, so I will not be explaining it in detail.

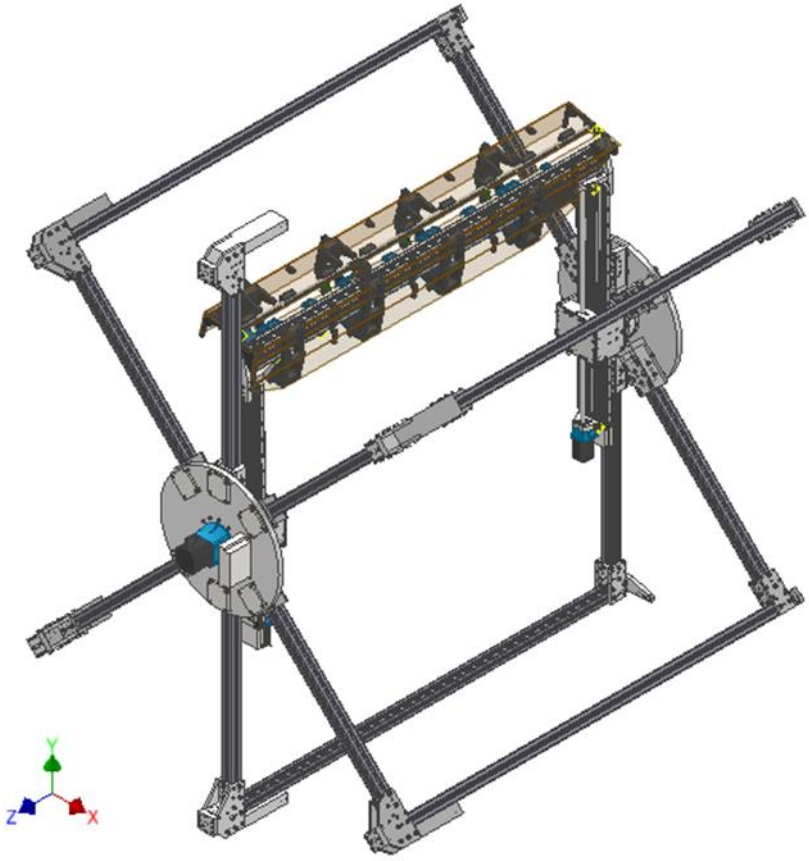

Fig. 14: SIT assembly

– **Y axis movement**

The movement in the Y axis ensures that, the SIT is able to achieve the insertion of the modules in every layer without a requirement of any manual changes to the structure. The largest diameter is 1275 mm and the smallest diameter is

600 mm, so the range of the Y axis movement must achieve at least 675 mm. Due to the visual input into the controls of the SIT, the movement must be very smooth, slow in order to prevent vibrations and the bluring of the picture (at leas for the “fine” positioning) and must have the ability to move in very small increments (0,01 mm).

– **Radial arm rotation**

This movement is required to achieve 180° clockwise and anticlockwise in order to reach every slot for the stave. The radial arm is unable to achieve the whole 360° turn, because it is limited by a number of cables constraining it. Due to this constrain, the 12:00 position was set as default for every stave insertion and the rotation is calculated from this position. The full 360° rotation is also not necessary due to the system of the stave inserting. Staves are not inserted in the full layers, but are divided into groups defined by the services (figure 15). After the whole group is installed, the services are connected and the nex group can be inserted. This process also added a new constrain. Because the installation of the services is done after a group of staves is inserted, the presence of a person inside the SIT are is required. Due to this fact, a request was made to avoid having a beam in the axis of the outer cylinder in order to keep as much free space as possible for the workers to install the services.

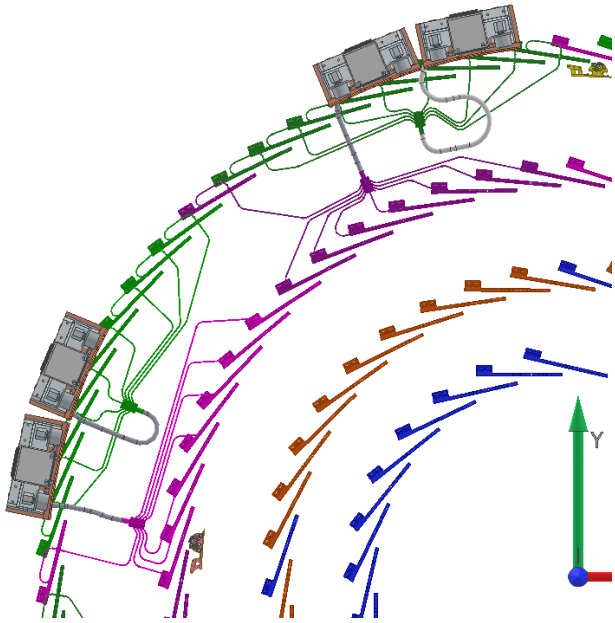

Fig. 15: Staves grouped by the services (green and purple pipes)

Another constrain was the 3.rd layer, where the box placed on the carriage colided with the longitudinal beam, used as a support structure for the inner side of the STI within the outer cylinder (figure 16).

Some of the brackets were covered by the vertical beams (figure 17), so the ability to remove the inner beams as well was required as well as the ability to remove the longitudinal beam which they originaly rested on.

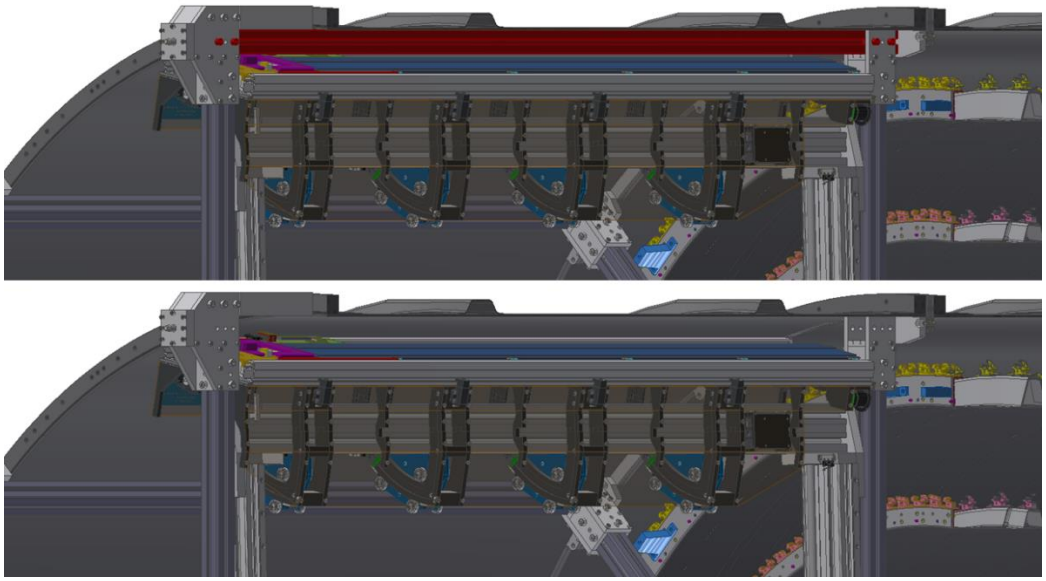

Fig. 16: Longitudinal beam (red) – with and without it

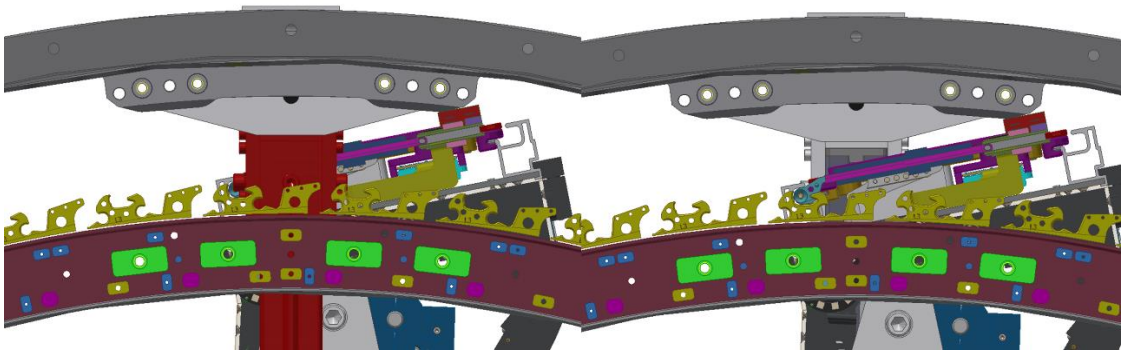

Fig. 17: Vertical beam (red) – with and without it

– **Carriage tilting**

The carriage tilting was probably the most challenging movement. This movement is crucial in order to fit all the staves inside the area. Because of the way the staves are stacked, they are tilted (see the chapter 1.1.1) diferently in specific layers, so the carriage must be able to achieve those tilts. It was also decided, it would be beneficial to achieve a position tangent to the outer cylinder axis in order to simplyfy the mounting of the box on top of the carriage.

The most problematic part of this task was the virtual axis of rotation, which had to be common with the axis of the bracked/stave rail (figure 18). To achieve this, a rounded rail was used, mounted with rolls on each side of it. The rails served

not only the purpose of the leads for the rolls, but also as the structural ribs, reinforcing the carriage.

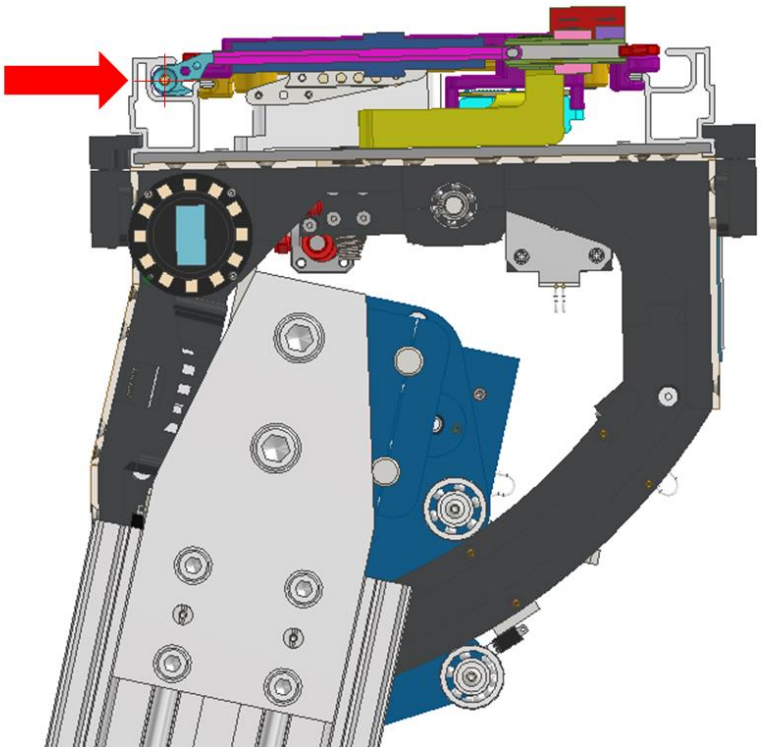

Fig. 18: the axis of the rotation (tilting)

– **Z indexing**

This movement serves to overcome the gap between the inner-most edge of the SIT and the outer-most edge of the barrel. This gap is left for the purpose of installation of the services. The issue of the Z indexing is that, the whole carriage must be able to achieve this movement uniformly, while also allowing the tilting.

– **Stave sliding (insertion)**

The stave insertion itself is the final movement in the sequence. This movement first requires insertion of a inserting pin into a slot in the stave structure and then a sliding movement along the whole length of the carriage. The default position of the insertion pin must be outside of the stave (pushed out), so there is no danger of the collision of the insertion pin with the stave during the installation of the transport box on top of the carriage. The movement must be very slow and smooth in order to prevent any vibrations and stress being applied on the stave itself. This process will be monitored by a force sensor installed and require the ability to stop and retract the insertion pin at any time.

2 Machine components for the prototype assembly

The market offers an abundance of components that could be used for the construction of SIT, therefore this research is limited to already selected types of components and specific parts and the justification of their choice.

2.1 Drives

2.1.1 Stepper motor

Stepper motors have the ability of microstepping, which enables very precise movements of the motor, which can be further enhanced by a suitable choice of transmission, or the pitch of the thread. Their controll is done by sending the information about the frequency of pulses and the direction of rotation by a control unit and subsequent positioning of the motor to the required position. An important specification of a stepper motor is the number of steps per revolution and the number of microsteps. This data indicates the number of positions of the stepper motor per revolution.

Stepper motors have a large starting torque, which in our case is a very desirable feature, because the tilting mechanism of the arm will be tilted in one position during the insertion of one layer, which represents a thret of mechanism freezing in that position. However, the high starting torque could compensate for this issue, but it is yet to be tested. The other possible solution of this issue is using one tier larger stepper motors. This feature makes the application of stepper motors a suitable choice for all axes. Specifically, the radial arm rotation requires a large starting torque due to the weight of the arm itself.

This type of motor can also be equipped with a brake, which will keep the motor in one position in the event of no current passing through it. This part turned out to be necessary for the motor mediating the rotation of the radial arm, where without a brake there was a spontaneous drop of the arm, especially in positions 3 and 6 (figure 19).

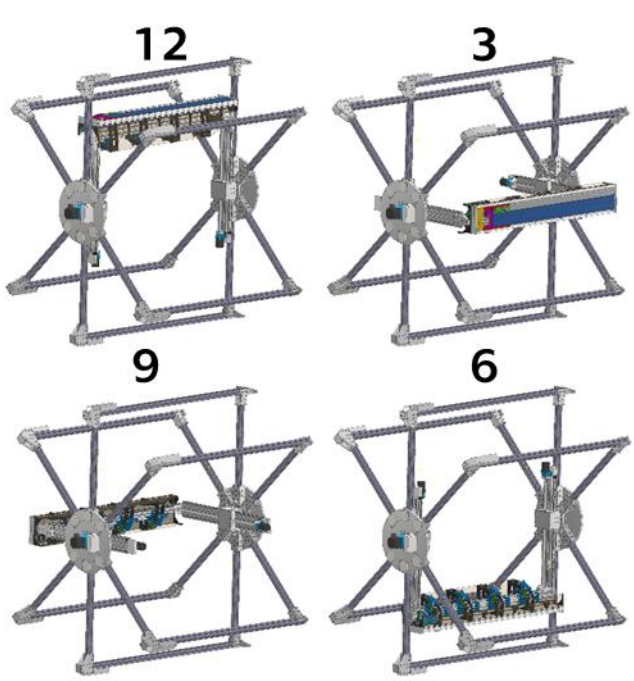

Fig. 19: Critical positions of the radial arm

2.1.2 Servomotor

Compared to stepper motors, servomotors are more complex devices consisting of a motor, a feedback sensor and a controller that controls the servomotor at the internal level. A fundamental advantage of a servomotor over a stepper motor is that it remains powered even when in a stopped position and is able to maintain this position and therefore does not require the usage of a brake in the event of a torque being applied to a stationary motor (e.g. position 9 and 3, figure 19). Another advantage is that, due to the nature of the servo motor, the position of the motor is always known even after the motor being disconnected from the power source. This feature allows it to be applied without using a default position with a limit switch. However, servomotors have a significantly lower starting torque and a very flat power curve. The fundamental disadvantage of servomotors is their price, which is many times higher than the price of stepper motors

2.1.3 Drives research evaluation

Even tho the servo motors seemed the obvious choice, because of their ability to keep the information of their last known position, after a careful consideration of functional and economic aspects, it was decided to use exclusively stepper motors, because we can compensate for the benefits of the servo motors in much more economical ways in the positions they are necessary.

2.2 Transmission

For the rotation around the axis of the outer cylinder, it was necessary to choose a suitable gearbox to achieve the required torque. The weight of the stave in the transport box was determined to be 15 kg, the weight of the arm (radial arm+ the horizontal beam) with the carriage was determined to be 25 kg.

$$m_1 = 15\ kg \qquad F = 400\ N$$
$$m_2 = 25\ kg \qquad M = F * s \quad (1)$$
$$m_c = 40\ kg \qquad M = 400 * 1 \quad (2)$$
$$s = 1\ m \qquad M = 400\ Nm$$
$$M_{1,2} = \frac{400}{2} = 200\ Nm \quad (3)$$

The minimum required torque is calculated for the third layer (the far most layer). Thus installing a gearbox will significantly reduce the size of the motor needed to achieve the required torque and significantly increase the positioning accuracy. The device will be equipped with a pair of gearboxes, so the torque applied on each of them will be $M_{1,2}$.

2.2.1 Worm gearbox

The fundamental advantage of worm gearboxes over other types is their self-locking, which would make allow the possibility to use a motor without a brake to rotate the mechanism around the Z axis. This would greatly reduce the noise of the device during rotation (the brakes on the motors tend to be very loud in high speed) and the control would be less complicated. However, the disadvantage of worm gearboxes is their size and weight, which would greatly increase the bending moment applied on the external attachment of the beams. Another disadvantage, which turned out to be a huge issue of the usage of a worm gearbox in this device, was the relatively large tooth clearances, which, especially in the positions 12 and 6 (figure 19), did not allow precise positioning of the stave. Since the arm rotates around the entire circumference, when moving from position 1 to position 72 and from position 72 to position 71, there would be a jump caused by the clearence and therefore a loss of the position (figure 20). A possible solution for using a worm gear would be to use a gearbox with a split worm. [5] [6]

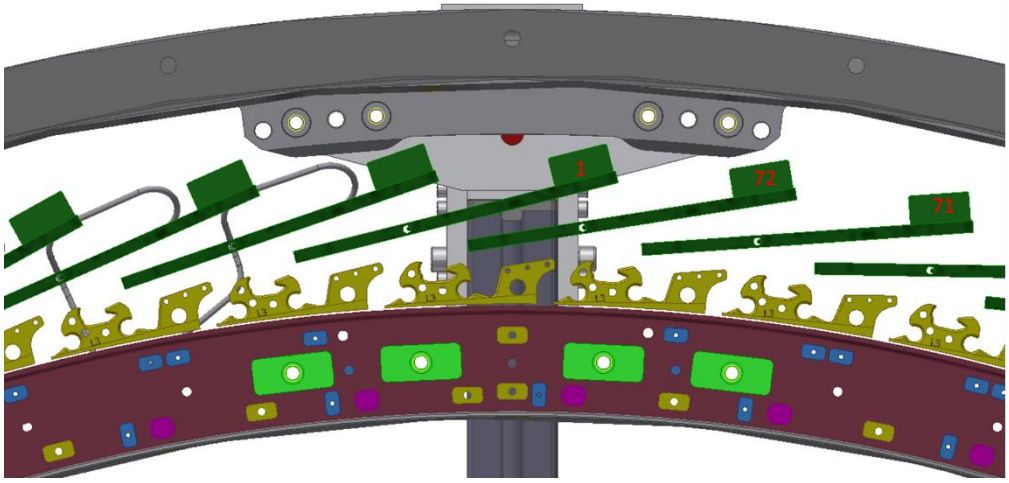

Fig. 20: Critical positions for the worm gearbox

2.2.2 Harmonic gearbox

Harmonic gearboxes are characteristic by their high rigidity, very small clearances, high efficiency, high load-bearing capacity and relatively small installation dimensions (they are flat in comparison to other types of gearboxes). Harmonic gearboxes are further unique being coaxial, which makes them a suitable solution for mediating the rotational movement of the arm since it is ideal to place the motor aligned with the axis of the outer cylinder.

Harmonic gearboxes are reducers. This is a special type of differential planetary gear with relative motion of the satellite on an eccentrically mounted input shaft of the gearbox.

In addition to the above-mentioned specifications, they are characterized by quiet operation, a small number of parts and the necessity of using a very low amount of lubricant, usually mineral synthetic oil or plastic lubricant.

As such, the gearbox consists of an elliptical wave generator, a flexible gear and a rigid gear. The elliptical wave generator is an elliptical cam equipped with a flexible bearing that deforms a flexible gear. A flexible gear is a flexible cylinder that has teeth on its outer side that mesh with a rigid gear when the cylinder is deformed. A solid gear is a rigid cylinder with internal gearing, with a greater number of teeth than a flexible gear. [7]

The harmonic gear principle uses different rotations of the outer and inner gearbox parts. The different number of teeth ensures the relative movement of the flexible gear to the fixed gear, which allows a high gear ratio to be achieved.

The disadvantage of using a harmonic gearbox is that they are not self-locking and it is therefore necessary to make up for this missing element (e.g. with a motor brake). [8] [9]

2.2.3 Evaluation of the gearbox research

Due to the very limited built-in dimensions for the SIT, it was necessary to use gearbox with an appropriate gear ratio and as small Z axis dimensions as possible, which is also able to transmit the required torque without the threat damaging the gearbox. At the outer end of the SIT, the larger size of the gearbox with the motor does not pose a problem, however the inner side of the SIT is limited by the detector barrel. Furthermore, due to the dimensions of the structure, the motor must be preferably placed in the Z axis, not next to the gearbox, which greatly limits the available variants. Although it was possible to find a worm gearbox on the market that meets the requirements, a harmonic gearbox seemed a more suitable variant because of its dimensions, coaxial properties and less vibration transmitted into the structure.

2.3 Aluminum strut profiles

Due to the design of the SIT, we resorted to using extruded modular aluminium profiles with T-slots, which offer a wide range of compatible fasteners. The advantage of these profiles is the ease of assembly without the need for profile modifications such as drilling or welding. The basic profiles are available in a wide range of sizes from 10x10 mm to 100x100 mm. However, in addition to square profiles, profile plates, double and reinforced profiles and stiff profiles are also available (figure 21).

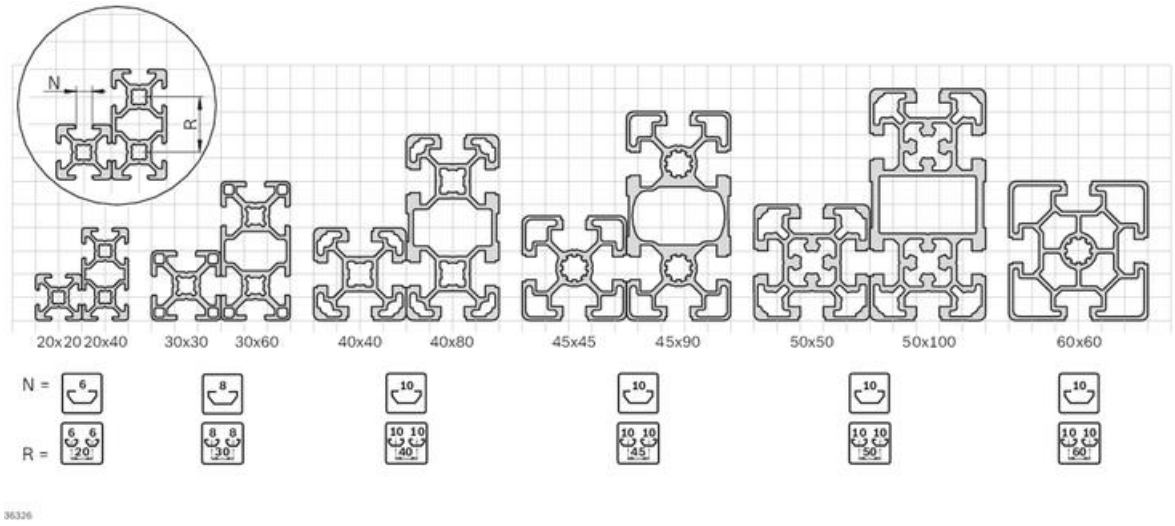

Fig. 21: Sample of T-slot profiles offered by Bosch [10]

In addition to profiles and fasteners, the manufacturers also offer a large variety of profile side caps or inserts into profile grooves for fixing panels (e.g. screen or plexiglass panel).

Due to the way these profiles are manufactured and their surface treatment, no machining of the profile surfaces is necessary and the length is very precise (±0,2 mm). [10] [11]

2.4 Axis guides

The designed device must move in several axes in sequence. To ensure smooth movement and minimize stress on components, it is therefore necessary to select the appropriate guidance method for each axis movement. I have specified the movements in more detail in chapter 1.3.

For straight-line guidance, only two options were essentially available for our purposes, namely the use of linear guidance with carriages, or the use of guide rods and the appropriate choice of bearings or slip sleeve bearing. In the following chapters I will discuss the available variations of the mentioned components and their combinations in more detail. Due to the geometry, the tilt arm guide had to be completely designed as no suitable variant could be found on the market that was also economically accessible.

2.4.1 Linear guide

The market offers a large variety of combinations of linear guides with trolleys that have a wide range of dimensions, starting at 4 mm rail width. The general advantage of linear guides is their relatively high load capacity, low footprint and high accuracy, while the disadvantage lies in their cost and their mounting, the accuracy of which defines the accuracy of the linear guide when multiple guides are used (especially parallelism). In addition, the linear guide can only be fixed by means of screws whose dimensions are proportionate to the dimensions of the guide and cannot be changed. This factor poses a problem for very small and very large lines. The use of a very small line in combination with an unsuitable base material, such as plastic, may result in insufficient strength of the thread into which the bolt is inserted and thus effectively reduce the load capacity of the trolley (or limit the load capacity of it by the load capacity of the threaded connection).

2.4.2 Guide rods

Another possible variant of the guide that seemed to be suitable for our purposes was the use of guide rods and a sliding element, i.e. ball or slip sleeve bearing. Compared to the linear guide, this is a more robust solution, as the smallest,

commonly available rods have a diameter of 8 mm or 12 mm, depending on the manufacturer and the required material. Given the number of parts used, the purchase price and the threat of contamination of the work place from lubricants were some of the relevant factors, because the insertion will take place in a clean room, where any environmental contamination is unacceptable.

Given the number of parts used, the purchase price and the threat of environmental contamination from lubricants were some of the most important factors.

Ball bushings reduce the friction by using a ball track that rolls down the guide rod. They have high accuracy, yet they do not reach the accuracy of the linear guides and are an affordable option. For use in the SIT, it would be necessary to select ball bearings fitted with seals to avoid the risk of damage (contamination) to the module from lubricant leakage. The disadvantage of the ball bearings compared to the sliding sleeve bearings is the relatively low load capacity and the need for regular servicing.

Slip sleeve bearings have a very low coefficient of friction and high precision. Compared to ball bushings, they are maintenance-free as their low coefficient of friction is due to the appropriate choice of materials from which they and the guide rods are made. Bronze and plastics with a low coefficient of friction (e.g. teflon) are most commonly used for their manufacturing and can be fitted with pockets filled with lubricant. The disadvantage of the slip sleeve bearing is that they have to be pressed into holes with prescribed tolerances, without which they do not have their sliding properties and precision.

Slip sleeve bearings have proven to be unsuitable for pressing into PLA, as the prints would need to be further processed after printing to ensure that the press holes meet the accuracy requirements. It would also be necessary to adjust the print parameters for the slip sleeve inserting, specifically increasing the perimeters of the hole walls and possibly thickening the infill around it. These tasks would further require testing for print optimization purposes, which would be time and material costly. However, for the use of ball bushings, a printed hole without subsequent modifications is sufficient and therefore, after evaluating the above reasons, only ball bearings were considered.

2.4.3 Evaluation of options for individual movements

High speeds of movement are not required for any of the axes and therefore this factor does not need to be taken into account in the selection process.

–Z axis movement

This movement is used to drive the arm into the layer position into which the segment will be inserted. A pair of electric motors with a trapezoidal thread was chosen for this movement. A pair of linear guides with a carriage was used as the guide for each of the two radial arms.

–Radial arm rotation

The radial arm rotation is used to position the carriage into the position of the groove for the insertion of the module. This motion consists of rotation around the axis of the outer cylinder along the whole 360° and is mediated only by the stepper motor and harmonic gearbox, with no additional guidance required.

–Z indexing

Z indexing is a movement that functions to bridge the services (cables and tubes) of already connected modules. It is the movement of the entire carriage in one axis by 120 mm. To achieve this movement, a system of guide rods was used on which the ribs with the tilting mechanism are seated. The entire arm is driven by a single stepper motor to ensure smooth operation and to keep the weight as low as possible.

–Tilting

Solving the carriage tilt guidance problem required several iterations of models and prototypes. As mentioned, the carriage must tilt in respect to a virtual axis of rotation. This condition required the use of rollers guided by a round groove. Here it was necessary to allow all the ribs of the arm to run smoothly at the same time, while still ensuring operation even when the arm was rotated in position 6 (figure 19). In order to ensure these characteristics, it was necessary to develop a mechanism that would allow the two parts of the carriage to be tensioned relative to each other, while keeping the weight of the arm to a minimum and therefore using the smallest possible tilt actuators.

–Rectractable pin guide

For the module retraction, it was necessary to develop a way to keep the clearance low to allow a controlled retraction of the module. However, the prototype design provided only very limited dimensions and required the lowest possible weight. The original design was for guidance using C-shaped bearings. However,

this solution involved placing too much weight on the horizontal beam, hence an increase in inertial masses on the rotation arm.

For the prototype, I therefore a linear guide was chosen, which is also produced in very small dimensions, resulting in a significant weight reduction compared to the above mentioned method. The linear guide has high precision and low resistance.

3 3D printing

3D printing, or additive manufacturing technology, is a way of part manufacturing, where the material is not removed, but rather added (layered). This technology offers, among other things, a possibility of rapid prototyping of shape-complex parts, the production of which would be very time-consuming and costly and sometimes even impossible with current technologies, and thus enables economical iteration of components before their mass production. This feature of 3D printing has been used extensively in the development of this device.

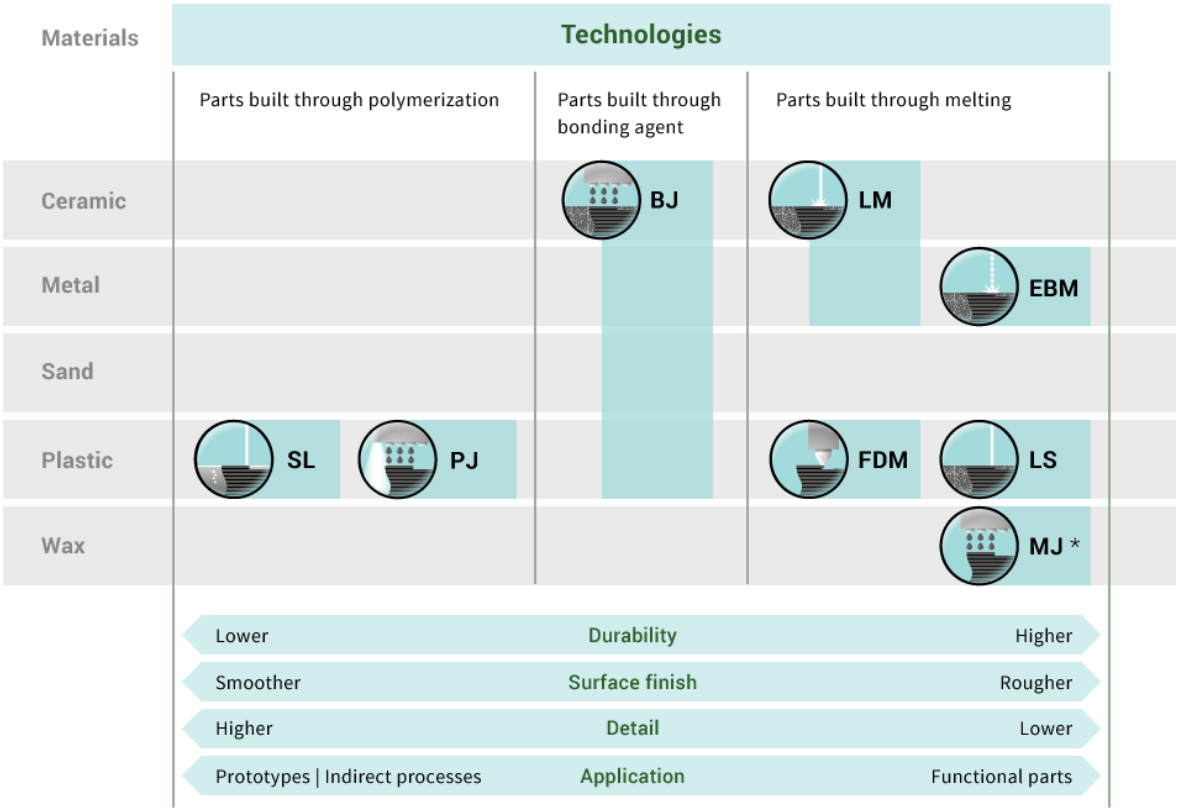

Fig. 22: Additive technology overview [18]

–**Stereolithography (SL)** is a method based on the curing of UV reactive resin in layers, using UV light. The print base is dipped into the resin and then irradiated. This method is very accurate and the prints achieve the same resolution as the display that irradiates the resin (currently up to 4k resolution). The special feature of this method is that, depending on the type of the UV source, it can cure the entire layer at once. However, despite this possibility, the production of the product is a very slow process and currently there is not a large enough variation of resins available.

–**Photopolymer jetting (PJ)** works in reverse to the stereolithography. In this method, the polymer is injected into a space irradiated by a UV lamp where the polymer solidifies rapidly. This method achieves similar properties to stereolithography, but printing in general takes longer.

–**Binder jetting (BJ)** involves injecting layers of binder between pre-prepared materials, which are either plates or powder, and then layering them. This technology works with a wide range of materials from paper to a variation of metal powders.

–**Laser beam melting (LM)** melting is a method of melting powder by laser in a single layer and then sintering additional layers. This process is carried out in a protective atmosphere and the product usually needs to be further heat-treated after printing is completed. This method makes it possible to process ceramic materials.

–**Electron beam melting (EBM)** works on a very similar principle to LM, but does not require a protective atmosphere and subsequent heat treatment of the product. Furthermore, this method is limited to metallic materials only.

–**Fused deposition modeling (FDM)** consists of melting a blank (string) and then layering the material on top of itself. This technology allows the production of products from the most commonly available thermoplastics. The production of products is relatively slow compared to conventional machining, but its main advantage is the acquisition cost and the price of individual products.

–**Laser sintering (LS)** operates on the same principle as LM, however, there is no complete melting of the material, but only a partial coating of the material to fuse it together. This method is suitable for the production of parts from commonly available thermoplastics.

–**Material jetting (MJ)** is used exclusively for the production of parts from wax and wax-like materials. The principle of this method is to spray liquid material in layers.

The overview and the figure 22 briefly sums up the available additive manufacturing technologies and their pros and cons. Due to the availability of the

technologies, FDM 3D printing appeared to be the most suitable method for prototyping atypical parts, such as a camera carrier or a rib arm tilting mechanism. [19] [20]

The principle of the FDM 3D printing is to stack layers of fused material (plastic), extruded through a heated nozzle, on top of each other to form a homogeneous structure. The disadvantage of 3D printing lies in the lower layer-by-layer durability and the visibility of the individual layers (which is only a aesthetical issue). It is therefore necessary to take these factors into account and to design and position the parts appropriately. Another problem of 3D printing that we had to deal with during the development of the SIT was the limited printing area of the 3D printer and therefore the limited size of the prints. This did not allow us to print some parts in their entirety, and it was therefore necessary to adapt the design to the possibilities that the laboratory had at the time. These factors led to gradual modifications of the models to the form in which they were subsequently installed on the SIT.

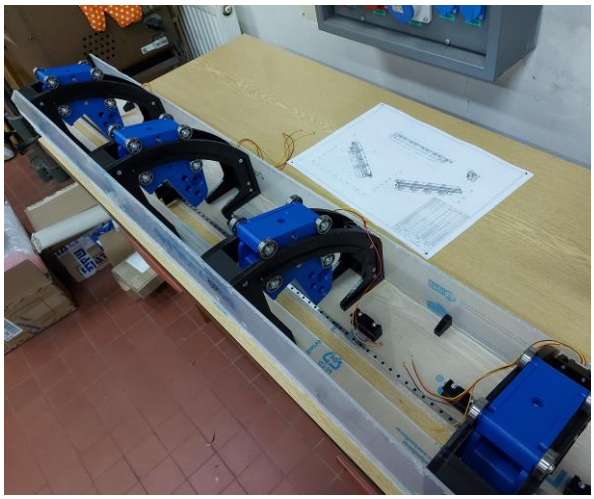

Fig. 23: The carriage assembly

Fig. 24: The rib assembly

Already from the boundary conditions defined by the client, it was apparent that the SIT could be composed without utilizing shape-complex parts, the production of which would require multi-axis machining equipment and the delivery time would most likely not allow sending the prototype to the RAL in Oxford for testing in time.

3.1 Materials

FDM 3D printing offers a wide range of usable materials, from which it is important to first appropriately select those that best suit the needs of the project. The Prusa MK3S printer was at our disposal, which in its basic configuration is

capable of printing a fairly wide range of plastic materials. This printer in the basic set up does not however allow printing of highly abrasive materials as it only has a brass nozzle which degrades rapidly when printing them (within hours/metres of filament) thus reducing the printing accuracy which is crucial for our purposes. This limitation eliminates all materials with carbon fibre admixture. These materials require a hardened steel nozzle, ruby nozzle, or other nozzle designed for printing abrasive materials. Furthermore, the printer in question does not allow printing of materials with high printing temperatures, such as peek, because the printer's hotend is not designed for temperatures above 300°C and the power supply does not provide sufficient power to heat the bed and nozzle for printing this material. I will therefore leave these materials out of the research. Moreover, I will omit all FLEX type materials from the research, which are flexible and therefore unsuitable for the prototype manipulator.

3.1.1 ASA

ASA (Acrylonitrile Styrene Acrylate) is an amorphous thermoplastic and was developed as an alternative to ABS. ASA is a material that is widely used in the automotive industry, where it is the preferred choice due to its weather resistance (mainly the wind). This material is also characterized by its high resistance to the UV rays. Furthermore, ASA has excellent mechanical properties that allow machining such as drilling or grinding. The material also has a high temperature resistance, where it can retain its mechanical properties up to temperatures reaching 96°C. The disadvantage of this material is that to achieve optimum printing conditions it is recommended to enclose the printer in a box where a constant temperature is maintained. In addition, the printout must be protected against draughts, as this could result in uneven cooling of the print and consequent curling. Another disadvantage of this material is its not insignificant shrinkage during cooling when printing larger areas (in standard FDM 3D printers this value can be up to 4% when printing an area of 220x220 mm). Using this material for prototyping purposes would be possible, however, the values we need for the manipulator are achieved by materials that are less demanding to print and their purchase price is significantly lower. [20] [21] [22]

3.1.2 ABS

ABS (acrylonitrile butadiene styrene) is a material very similar to ASA but does not have such high impact and UV resistances. Like ASA, ABS can be easily smoothed using acetone or acetone vapor to achieve a smooth surface (hide layers). Unlike PETG, it can be easily machined (grinding, cutting, drilling, etc.).

ABS, like ASA, has a high thermal expansion and the print therefore shrinks by up to one percent after cooling. However, printing ABS is a rather demanding process, and apart from maintaining a stable temperature throughout the print and protecting it from draughts, it is necessary to use a separation layer on the print bed to prevent damage during print removal. This material is unsuitable for our purposes due to the difficulty of printing and the cost of the material. [20] [21] [22]

3.1.3 Nylon

This material is very strong and flexible and has a high resistance to abrasion. The material does not shrink when cooled, but it is very vulnerable to the air moisture, which it absorbs. Printing nylon is problematic due to this property and it is recommended to keep the filament spool in a so-called dry box (a storage space with very low air humidity, usually equipped with a system to reduce it - silica gel, heating element with fans, etc.), which the laboratories of the Institute of Design and Machine Parts of the Czech Technical University do not have on their disposal. [20] [21] [22]

3.1.4 Recyclates

Recyclates such as rPET (recycled polyethylene terephthalate) are recycled materials. This material was developed primarily in an effort to recycle plastics and therefore reduce the plastic waste produced by the 3D printing industry. It is created by mixing shredded recyclate and new plastic pellets that are used to produce the new material. Recycled materials are usually lower in cost and tests show that they are more durable than PLA, mechanically, chemically and slower to degrade to UV, but do not achieve the same values as, for example, PETG. However, these materials are generally difficult to print and the print quality (mainly stringing quality) is inconsistent across the spools, making them unsuitable for our purpose. [20] [21] [22]

3.1.5 PETG

PETG (Polyethylene terephthalate Glycol) is a thermoplastic that forms a compromise for 3D printing between the easy-to-print PLA and more demanding but mechanically more resistant materials such as ABS. PETG has a higher melting point than PLA and is much more resistant to UV radiation. This material absorbs virtually no air humidity and is therefore, unlike PLA, suitable for use outdoors without surface treatments (painting). Although the PETG is generally considered to be a class above PLA, it does not achieve the same resistance to abrasion. A further problem lies in the surface finish of this material when a smooth wall is required.

While PLA can be easily smoothed with chloroform fumes, PETG cannot be smoothed with any chemical (a commonly available chemical under safe conditions). Furthermore, mechanical finishing of an already printed part is highly problematic as the material tends to melt and clump, making grinding highly problematic. [20] [21] [22]

3.1.6 PLA

PLA or also polylactic acid is a material made primarily from corn or potato starch. This material holds together well, the layers easily stick together and does not tend to shrink after printing. This feature ensures very accurate printing (within FDM printing), making it a very suitable choice. The material is more brittle than PETG after printing, but is much more resistant to abrasion. Another characteristic of PLA that was critical to the choice of material for our purposes was the minimal tendency for the print to curl during the cooling of the layers. This phenomenon occurs due to internal stresses, which increase as the number of layers increases and can lead to tearing of the print from the print base. This material can be smoothed with chloroform or chloroform fumes.

The disadvantage of PLA is the tendency of the print to absorb air moisture and subsequently form bubbles on the surface of the material, which in turn affects the overall accuracy of the print. This process can gradually degrade the material so extensively that the print may crack and become mechanically damaged. However, this process takes a relatively long time (years) even in very humid environments, which the manipulator should never enter, and this characteristic is therefore not an issue for our project.

Another of the undeniable advantages of this material is its price, which places it among the most affordable materials currently available.

PLA is divided into PLA-A, PLA-D and PLA+, which differ mainly in printing properties and have different toughnesses. For our purposes, however, standard PLA (PLA-A) is sufficient [20] [21] [22]

3.1.7 Evaluation of the research of available materials

From the available materials, it was first necessary to eliminate materials that did not have the required mechanical properties (stiffness and resistance to abrasion) and materials whose print quality was inconsistent at the time of production. Subsequently, the most suitable material had to be selected from the remaining materials (PLA, ASA, ABS, Nylon). Furthermore, the selected material should not tend to wrinkle during printing and the final product should not shrink after printing to reduce the design effort of the parts and eliminate the need for

shrinkage compensation. Last but not least, because of the number of parts and their iterations, the economics of materials must be evaluated.

Of the materials mentioned above, only Nylon and PLA have the aforementioned properties. Despite Nylon's tendency to absorb airborne moisture, it appeared to be a suitable candidate, as at the rate of material consumption, the filament would not have the ability to absorb moisture in such a short period of time. Thus, the final deciding factor that ultimately led to the use of PLA was the cost, which for PLA is approximately half of the price of Nylon. [20] [21] [22]

3.2 Print settings

Another important factor in 3D printing is the optimization of the part itself, both in terms of shape and in terms of the print preparation in the slicer. In order to achieve a higher stiffness of the part, it is necessary to choose the correct fill density and number of perimeters. The number of perimeters has proven to be a very important parameter during prototyping, as a low number of perimeters not only makes the print softer, but can also cause the edge of the infill to push through the side wall of the print and consequently create unwanted relief on the outer wall of the print. This problem has proven to be particularly significant when printing ribs that act as guides to guide the tilting mechanism of the arm. The pushing of the infill through the wall and the subsequent formation of the relief did not allow smooth movement of the rollers and resulted in vibrations and, in extreme cases, jerky movement.

Once the material has been selected, the printer must be calibrated for the material, specifically setting the correct print temperature, print speed and retraction to achieve maximum accuracy. If the temperature is set too low, the material will not melt enough, so the layers and perimeters of the print will not bond well enough and the print will not behave as a homogeneous structure and will tend to break up layer by layer. On the other hand, if the temperature is set too high, the product will melt and will not have sufficient precision and the desired mechanical properties. Print speed is also an important parameter, which is mainly influenced by the complexity of the parts. If the part is complex in shape and contains many retractions, it is necessary to take this factor into account when setting the print speed, as it could lead to the formation of strings (threads of melted material) that drag behind the nozzle and can either stick to the print or get caught on the nozzle, where the accumulated filament then forms a drop. If too large of a droplet falls onto the printout, it may collide with the nozzle after it has cooled down, causing the print to fail.

4 First SIT assembly iteration

Many iterations of individual SIT nodes preceded the final version of the model. For ease of orientation, I have divided the SIT into several subassemblies that provide the corresponding motions (section 1.3).

In this chapter, I describe each node in detail and present several iterations of it, along with the problem that caused the change. As can be seen from the following paragraphs, the carriage had to be optimized for the required stiffness while maintaining the minimum mass, which has a major effect on the inertial forces during rotation of the arm and therefore on its accuracy and repeatability.

4.1 Outer frame

The outer frame of the SIT consists of two opposing central hubs (figure 24) with six beams, which are identical, mirror-reversed and differ only in the area of the anchor point nodes. The outer frame also includes the longitudinal beams and the fitting for those beams.

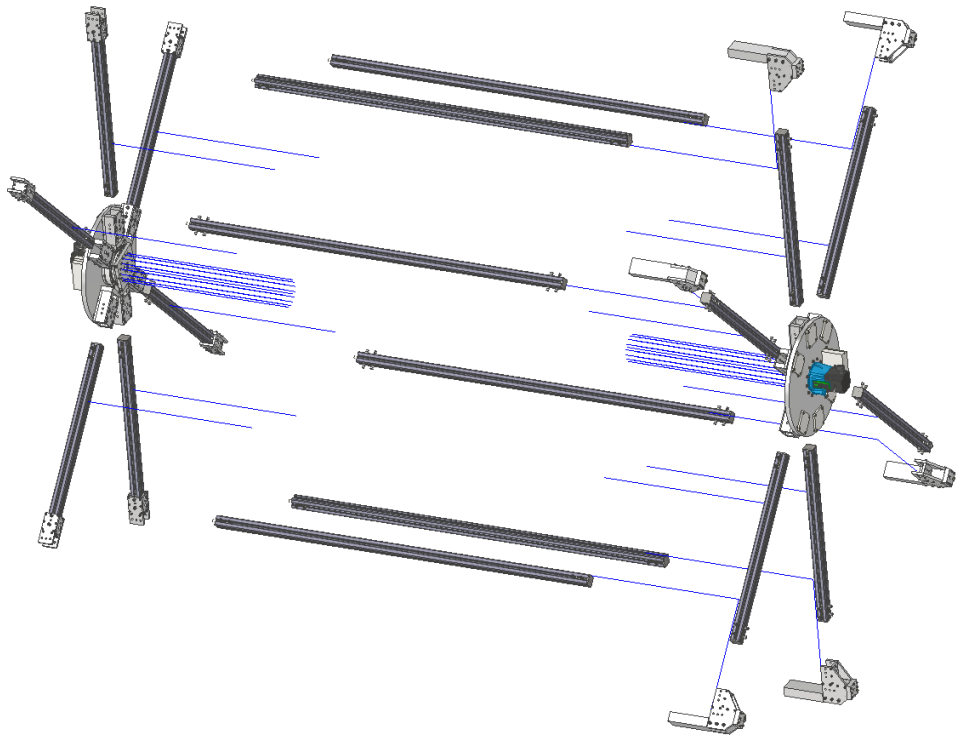

Fig. 24: Outer frame

4.1.1 Central hub

The central hub consists of the six beam mounts, the gearbox, the plate carrying the sliding of the radial arm mechanism (Y axis movement, chapter 1.3),

the engine carrier with the engine fitted with a flexible coupling and the central plate (figure 25).

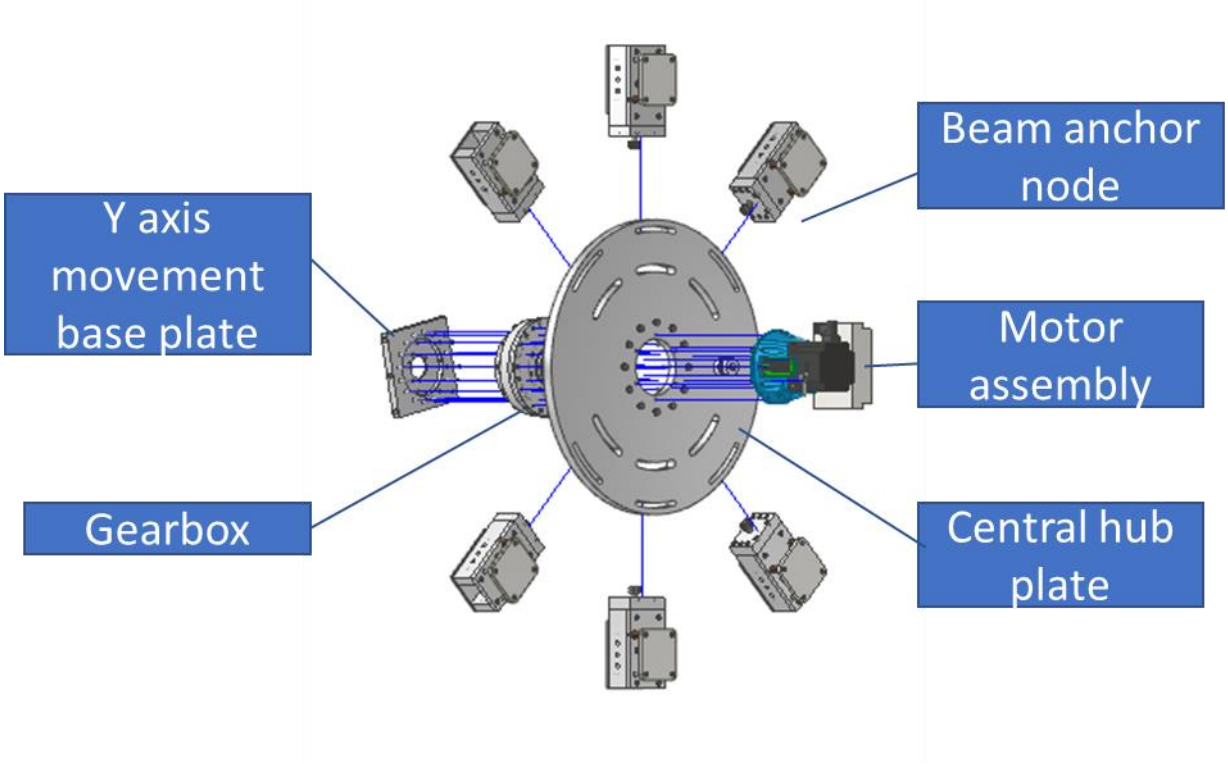

Fig. 25: Central hub

The central hub serves as a carrier for the rotating mechanism (motor with brake and gearbox) and also as a support for the beams. Due to the dimensions, it was necessary to design a system that would allow the central hub to be moved and thus ensure the alignment of the device. This was achieved by a combination of cut-outs in the plate and the beam fits (figure 26), which are housed in these cut-outs. This mechanism allows the centre to be moved freely (within range) and thus ensure the alignment of the two central hubs with the outer cyllinder.

The beam placement is connected to the circular plate by a pair of screws and the clearance is defined by guide pins, which are inserted in the guide pin hole. The assembly is further provided with a set screw which indicates the length of the beam and thus changes the position of the centre. After calibration of the device, the beam fit is tightened against the circular plate by four screws, thus defining its position. In the next step, the rest of the screws that define the position of the beam are tightened (figure 27).

The final version of the manipulator will be fitted with a housing for the use of the laser system and apertures to control the alignment of the mechanism.

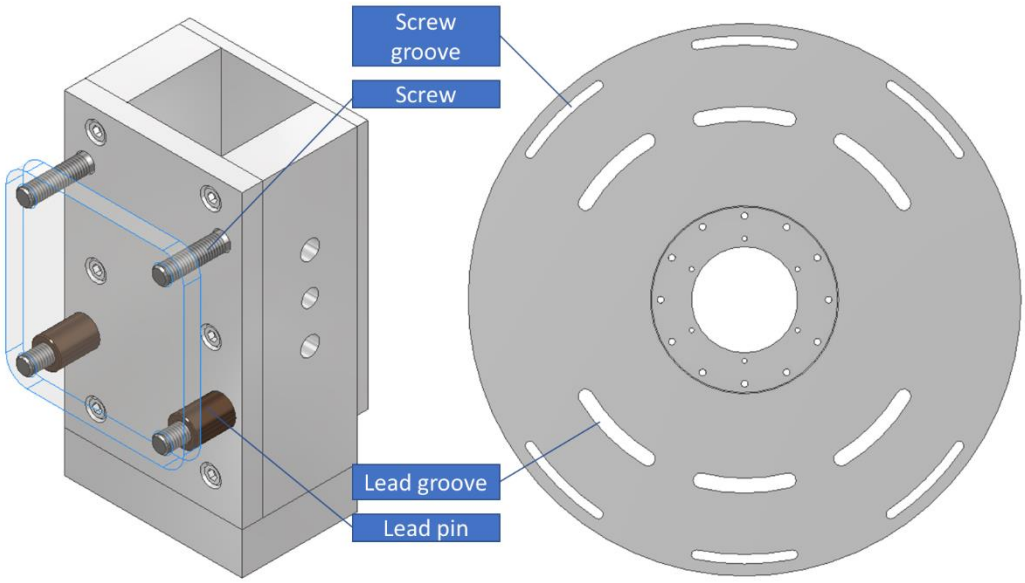

Fig. 26: Central hub positioning assembly

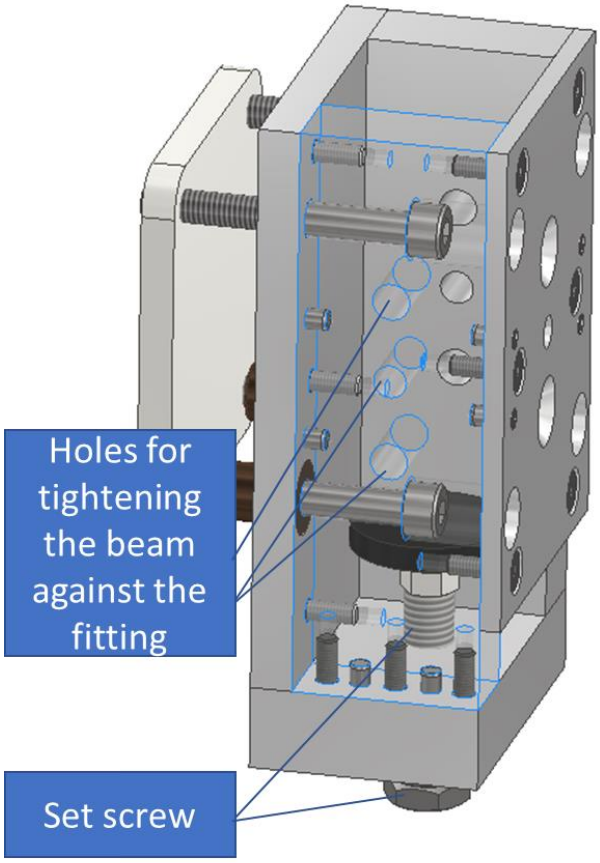

Fig. 27: Beam anchor node

4.1.2 Beams anchoring to the outer cylinder interface

The beam placement had to be somehow relocated on the inner side of the outer cylinder (figure 28), as the position of the anchor points on the perimeter of the outer cylinder is too deep to place the central hub directly, because the SIT would interfere with the space dedicated to services for the maintenance and function of the modules. However, simple offsetting was not possible due to the requirement for the individual legs to be removable. During the assembly/disassembly of the beam, due to the poor access and the very small distance from the outer cylinder, the disassembled beam collided with the wall of the outer cylinder and threatened to puncture it. The stability of the assembly proved to be another problem, as the removal of one of the legs with the offset resulted in deformation of the structure and bending of the other offset legs. For the reasons mentioned above, it was decided to use a horizontal beams extending along the entire length of the outer cylinder instead of using a separate part to carry out the anchor points (figure 28, red).

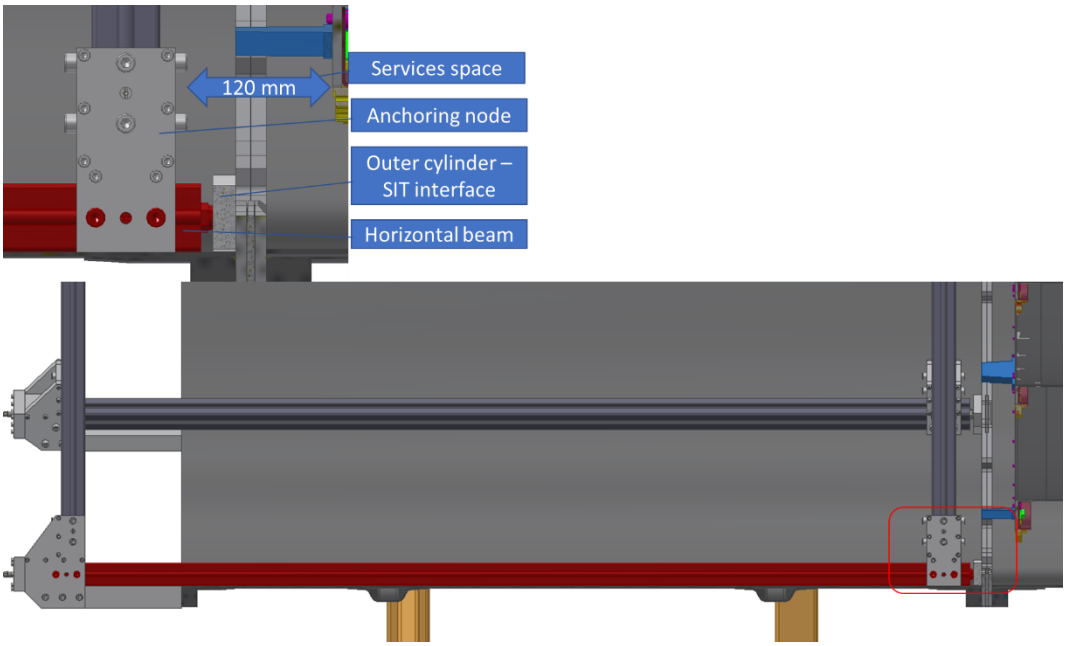

Fig. 28: Internal fitting detail

However, the beams collided with the box in which the module is stored during the insertion of the specific modules (figure 17) and therefore it was necessary to allow their removal. This modification forced the modification of the sockets on the outside of the outer cylinder to the form shown in figure 29. The mentioned sockets are fitted with a through-hole so that they allow the beam to be slided outside of the outer cylinder. The only disadvantage of this solution is the necessity of a space behind the manipulator of a minimum length equal to the length of the beam. The

sockets are also fitted with a removable threaded plate which serves as the end of the slot of the horizontal beam and is also fitted with a set screw which allows it to be tensioned against the anchor point on the central hub.

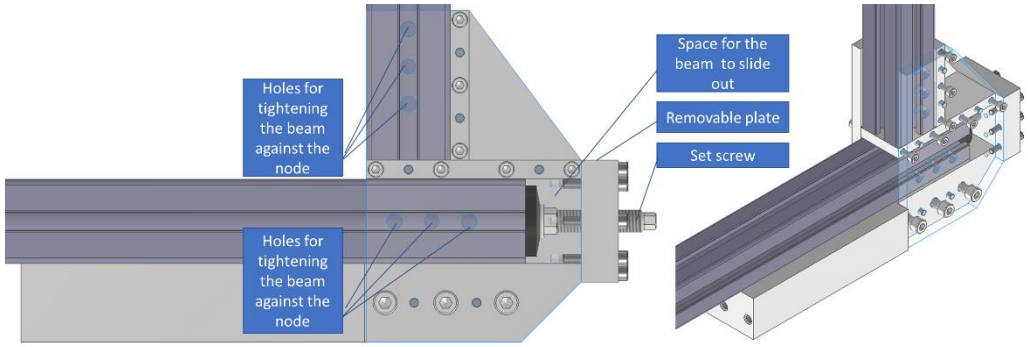

Fig. 29: Outer anchoring node

4.2 Arm (carriage) support structure

I referred to the pair of the radial arms, connected with a horizontal beam as arm support structure, a part of the device shown in figure 30. The function of this structure is to carry the weight of the carriage and module in the transport box and to provide the movement along the Y-axis. As can be seen from the aforementioned figure, the basis of this assembly is three beams. The side beams (radial arms) serve as the base for the sliding mechanism that provides the Y-axis movement. While the top beam serves to accommodate the carriage.

Fig. 30: Arm (carriage) support structure

4.2.1 Y axis movement

The movement along the Y axis is achieved by using two motors on which a threaded rod with a trapezoidal thread is connected using a flexible coupling. The mechanism also includes a housing (figure 31), fitted with a pair of nuts which are tensioned against each other by a trio of bolts. Another essential part of the mechanism is the linear guide, which protects the threaded rod from deformation and ensures that the mechanism runs smoothly along the set trajectory in all positions of the insertion process. The housing is also connected to the carriages of the linear guide on one side, and on the other side it is bolted directly to the harmonic gearbox by means of a support plate.

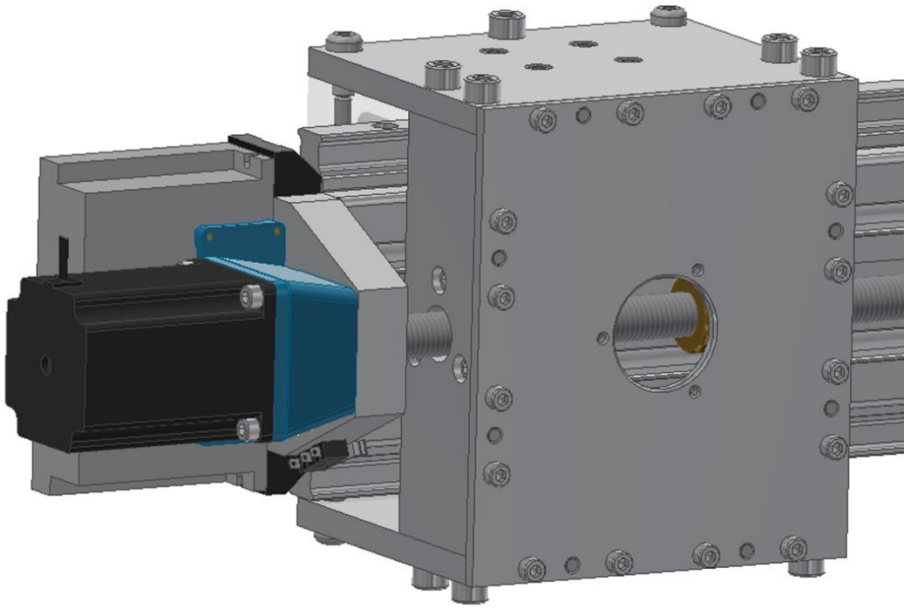

Fig. 31: Y axis movement mechanism housing

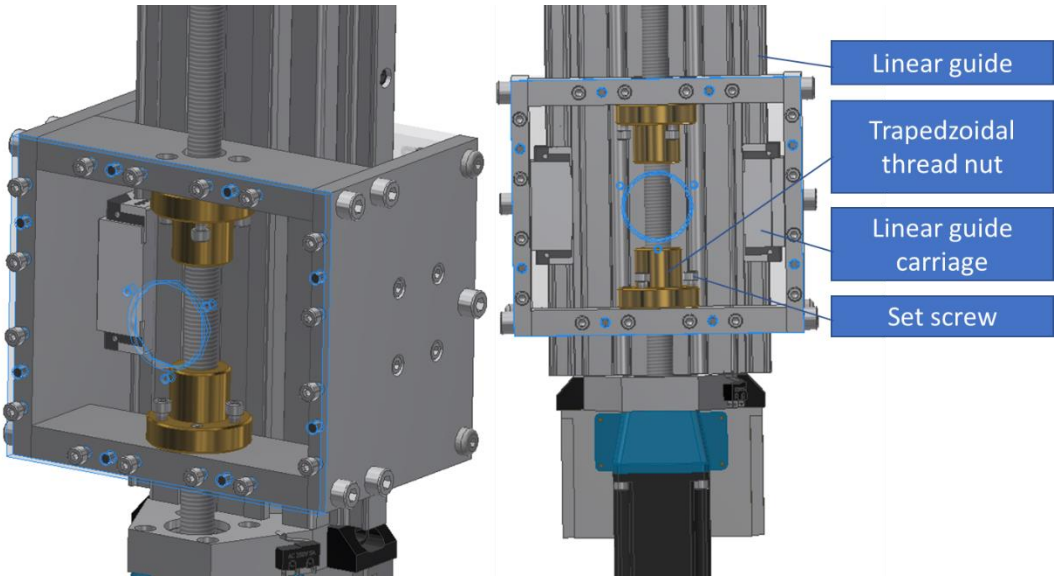

Fig. 32: Detailed Y axis movement mechanism housing view

4.3 Arm

The part of the SIT, I have referred to as the arm, consists of the carriage, its guide rails and the beam it is mounted on. It is the most complex part of the SIT and has to perform several movements. I have divided into a tilting mechanism, a mechanism for pin movements and Z indexing. The carriage also carries the camera, which controls the “fine” positioning of the arm and confirms its position

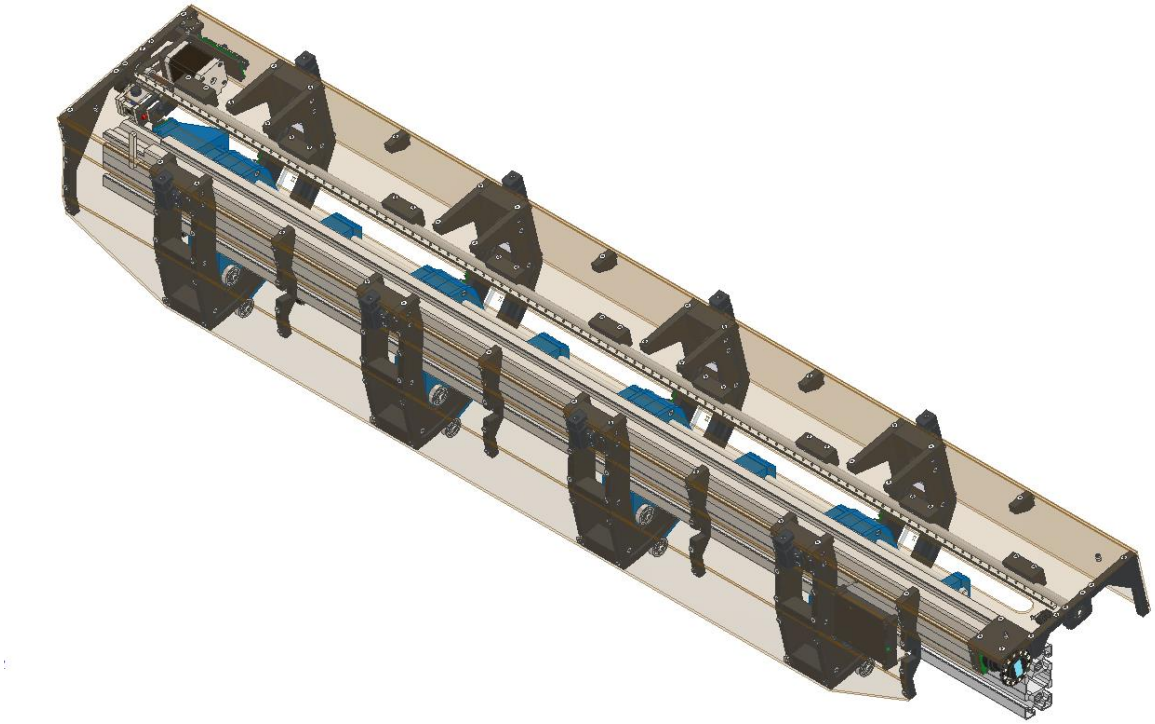

Fig. 33: Whole arm assembly

4.3.1 Z indexing

Z indexing is a movement that provides the bridging of the services (the cables of already inserted modules). This movement must be performed by the entire carriage, as tilting is the last movement before the module is actually inserted. It therefore means that the carriage must be designed as a shell on which other elements are consequently placed.

The whole carriage is moved by a single motor, which is fitted with a threaded rod and is only connected to the arm by a nut embedded into the first rib. Furthermore, it was necessary to develop a system of rails that would ensure a smooth movement of the arm in all positions and maintain its rigidity (no bending/buckling). Thus, a system of guide rods and linear bearings was designed for the guide. The system consists of two continuous rods (red) that serve as guides and are firmly connected to the beam that carries the entire carriage. In addition, there are three spacer bars (pink, green, yellow) on the assembly which are rigidly

connected to the arm and are connected to the beam only by bearings 5, 6 and 7 (figure 34).

Fig. 34: Guide rods system for the carriage

A pairs of bearings 1-4 are mounted in the outer shell of the carriage. This system allows a total maximum displacement in the Z-axis direction of 120 mm, which is defined by the spacing of the ribs. In addition, smooth movement and high rigidity are ensured in this way. This guide bar system is the only supporting the structure of the carriage holding the stave in the box.

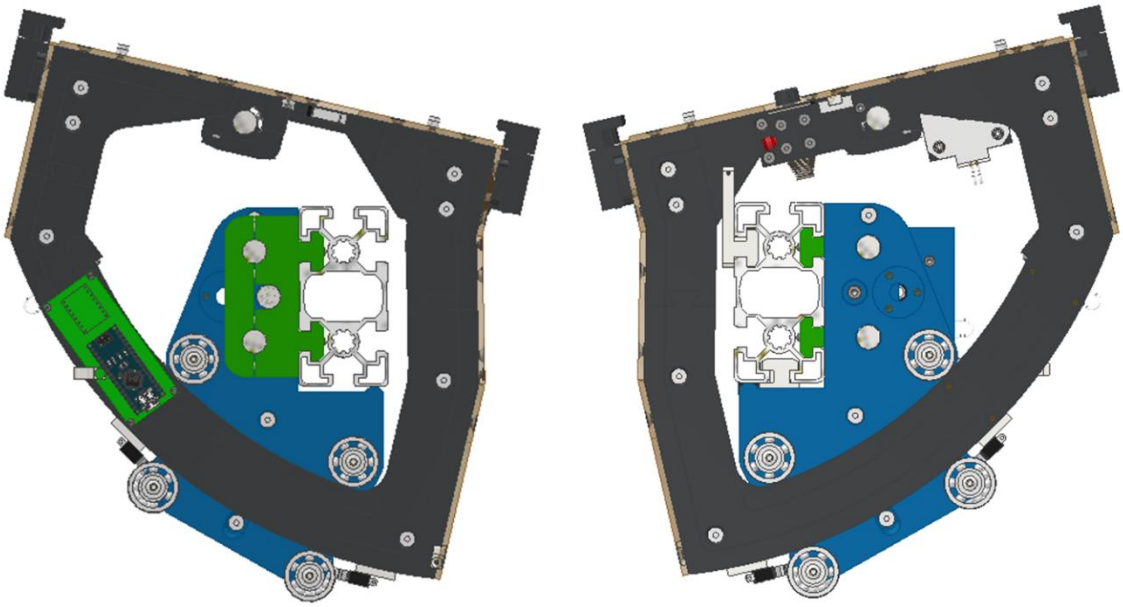

Fig. 35: Front and back view of the ribs assemblies, mounted on the horizontal beam

As can be seen in the figure 35, the roller assembly (blue) is only connected to the beam by guide rods, which are attached to the beam by carriers (green).

4.3.2 Carriage outer frame

The entire carriage outer frame had to be designed so that it could be mounted on the bearings of the previously mentioned guide rods (chapter 4.3.1). Due to the length of the arm and the effort to keep the weight as low as possible, the arm was made of four ribs, which are primarily made of low-fill printed parts with an increased

number of perimeters, which reduces the weight and at the same time provides sufficient stiffness in the direction in which it is required. The ribs are joined together only by the polycarbonate plates that form the outer shell and a single guide bar between each rib that acts as a spacer. This rod is held in place by a linear bearing to reduce its deformation to minimum and also add as low friction as possible.

The polycarbonate plates are then bonded at 6 points with printed parts to increase the stiffness of the outer shell. The use of a composite shell was also considered, but this option was abandoned as it was anticipated that the current design of the shell was a first iteration rather than a final design. Another factor was time, where the delivery time of the composite shell could be up to a few months, and last but not least the price, which would exceed the price of polycarbonate plates many times over.

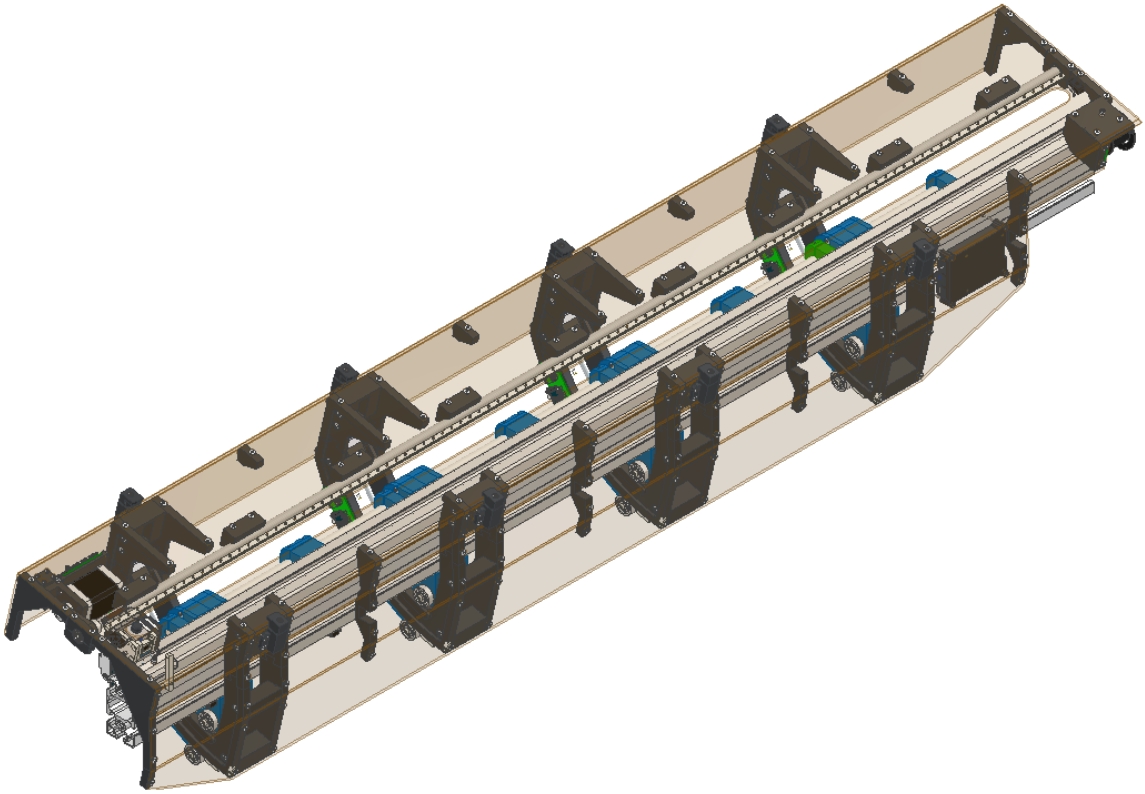

Fig. 36: Carriage

4.3.3 Ribs

As already mentioned, the carriage is made up of, among other things, four ribs that serve as a guide rail for the rollers placed on the printed assemblies (figure 37).

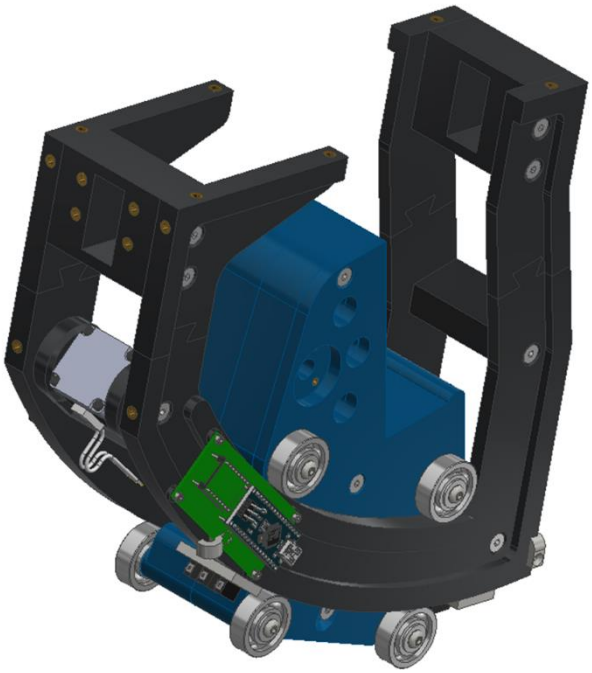

Fig. 37: Rib assembly

The ribs also carry the actuators that allow the carriage to be tilted to allow precise positioning of the Staves. As seen in Figure 38, the ribs do not have a flat backside. This shape was given by the required tilt range of the module, which was from 0° to 13°, and a 90° arc was not sufficient to achieve this range. Although the staves will only be retracted in 11° 12° and 13° tilt positions, the 0° tilt position is beneficial for mounting the transport box on the arm and securing it, which will occur at the 12:00 position.

After a brief consideration, the range was increased to 0°-15° in order to allow compensating of the inaccuracies.

Fig. 38: Rib assembly in minimum and maximum tilt position

The shell of the carriage has to be open on the underside (figure 35), which greatly reduces its stiffness, and to compensate we were forced to increase the thickness of the ribs to increase their stiffness.

In the figure 39 it can be seen that the assembly is made up of two parts with rolls (blue) and a pair of guide ribs (black). The blue parts are connected together by a bolt, which also serves the purpose of pretensioning the rollers against each other. The black parts then form the support for the envelope of the carriage. It can be noted further in figure 39 that each rib assembly is provided with a single stepper motor providing the tilting of the arm. The motor and nuts are arranged to allow smooth movement of the rib along the full range of its positions.

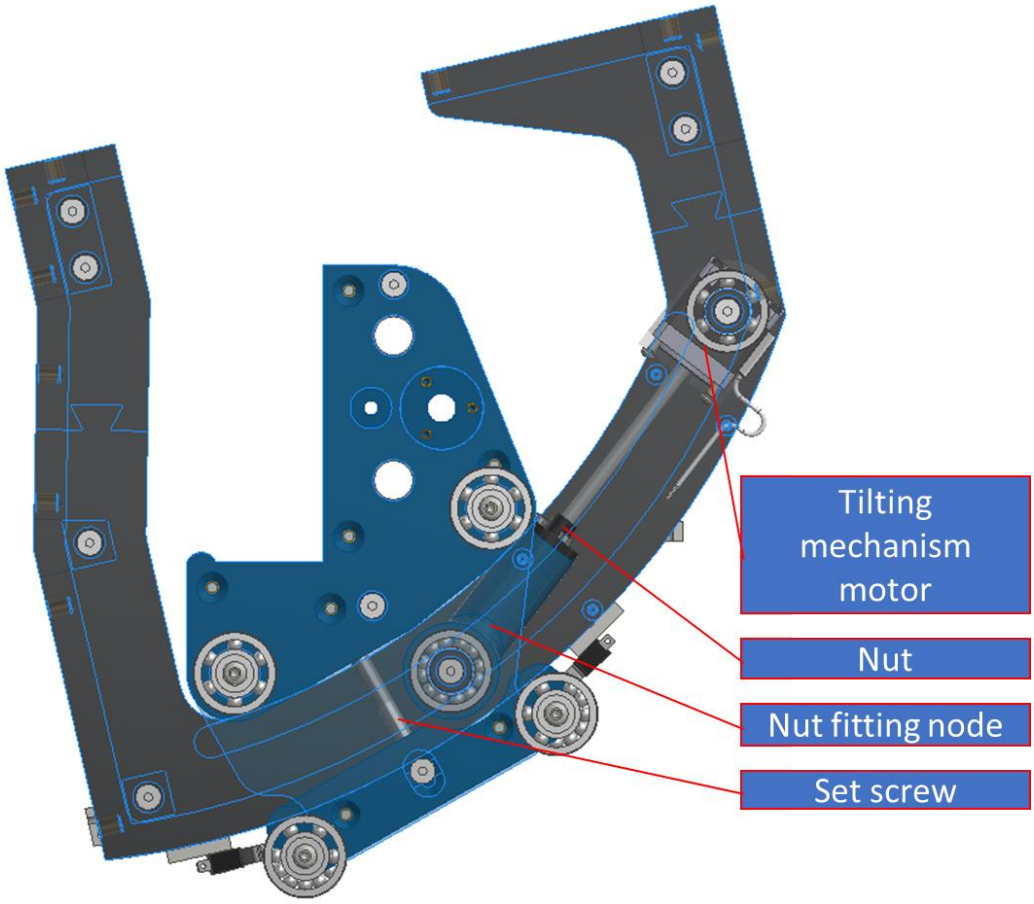

Fig. 39: Tilting mechanism

4.3.4 Stave insertion mechanism

Another movement that we had to incorporate into the carriage and which had to move with the Z indexing was the insertion of the strip using a insertion pin. This was achieved by placing the mechanism on the bottom of the top plate of the outer shell.

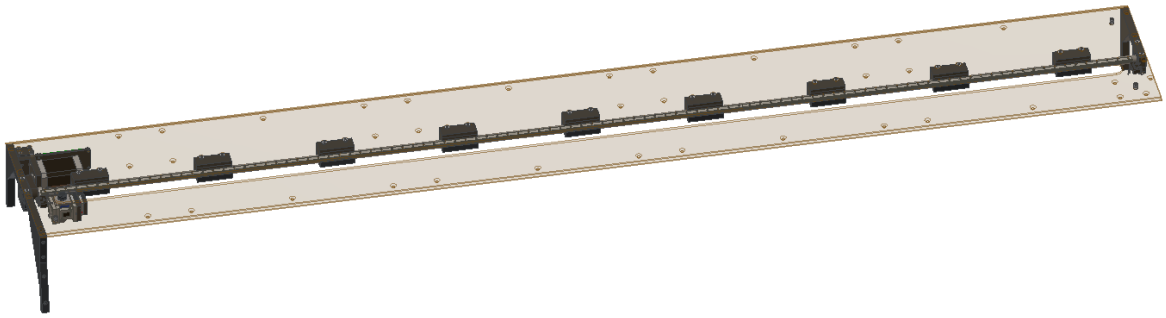

Fig. 40: Top plate assembly

The requirements for the pin were that its default position had to be retracted so as to prevent any damage to the stave in the event of a loss of power due to the pin driving into the uncovered part of the stave. This was achieved by using an electromagnetic pin, for which we reversed the sense of its function by a slight modification.

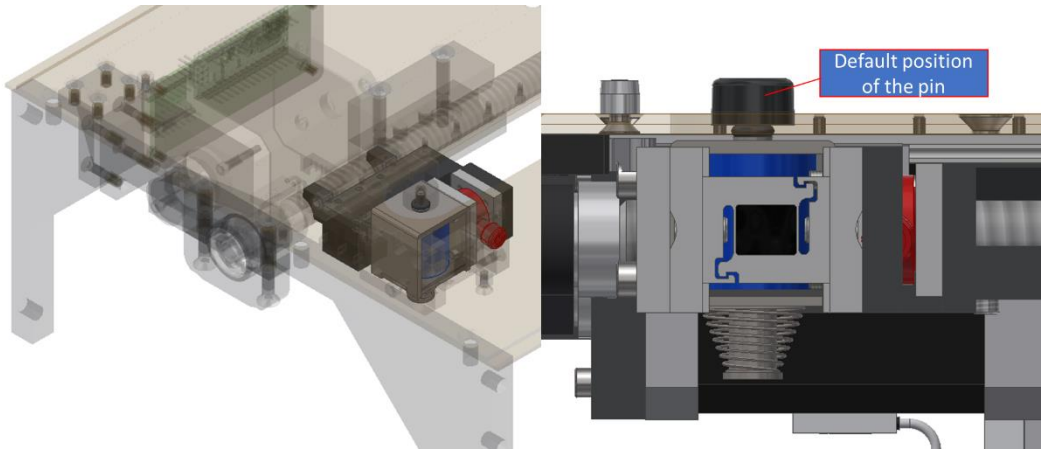

Fig. 41: Default position of the insertion pin (retracted)

However, the control and the power supply of the insertion pin proved to be problematic, as the trolley with the pin must travel a distance of 1500 mm, but no cables are allowed to hang freely from the carriage, as this could cause entanglement and damage to the device. It would also present a risk of an injury for the operators. To solve this problem, it was necessary to replace the straight cable with a twisted cable that is centered by a guide wire. This ensured that the cable was long enough to reach the desired position, while at the same time preventing the cable from hanging loose due to the gravity.

Another node of the insertion mechanism was the movement of the pin along the length of the arm. This movement is, as already mentioned, 1500 mm long. A large number of designs have been evaluated to provide this movement, however,

they either involved adding too much weight to the carriage and consequently increasing the inertial masses, or did not provide sufficient accuracy. Designs included various variations of guide rods, but these presented too much weight and further required relatively large clearances. Other designs included the use of belts and chains, but their major disadvantage was their deflection in certain positions and hence inaccuracies that could not be compensated for as they varied for each position of the arm. At first it seemed possible to solve this issue by using a tensioning mechanism, but this solution proved to be very problematic while maintaining the existing dimensions of the arm. The final design that was implemented was the use of a linear guide of very small dimensions and a trapezoidal bolt, between which a carriage with a 1/4 brass nut is spaced.

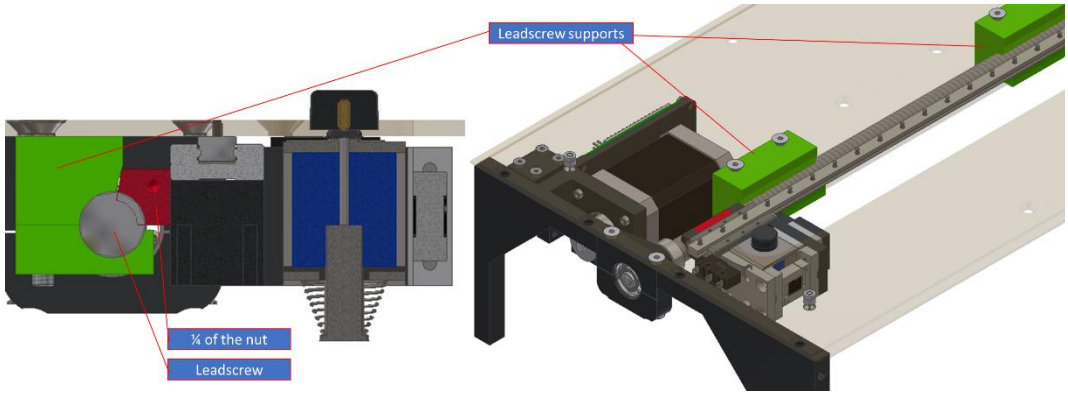

Fig. 42: Stave insertion mechanism

As figure 42 shows, the piece of the nut performs the function of a standard nut, however, due to the lack of space and the need to support the threaded rod, the nut had to be reduced to a comb, which, due to the rotation of the trapezoidal bolt, moves the carriage with the pin to which it is attached. On the opposite side of the threaded rod the supports of the threaded rod can be seen, which prevent its deformation in critical positions and allow the nut to move freely.

5 Design optimization

Based on the knowledge gained from testing the first version of the SIT, it was necessary to optimize the design. It turned out that some of the originally designed motors were not able to provide a smooth enough movement and the assumed rigidity of the structure was not sufficient in some places. Furthermore, it was decided that the manipulator control, which was originally based on the Arduino system, would be redesigned to an industry standard. This meant creating new pathways for the cables, the design and installation of their carriers and the carriers for the electronics themselves. The topic of control is not discussed in this thesis, as it is not the subject of this thesis.

The external shell of the manipulator provided sufficient rigidity, however working with the vertical beams proved to be quite problematic and adjusting the alignment of the central hubs was uneasy due to the high number of moving elements. For this reason, it was necessary to develop a new system that retained the ability to adjust the alignment but was less complicated. It was also necessary to create elements for the placement of the alignment control system (laser, aperture and sensor).

5.1 Central hub alignment update

The central hub has undergone a complete rework. The alignment of the two central hubs has been greatly simplified, which is now mediated by four screws for each central hub, that limit the movement to only two axes but maintain a circular field in which the axis can be moved.

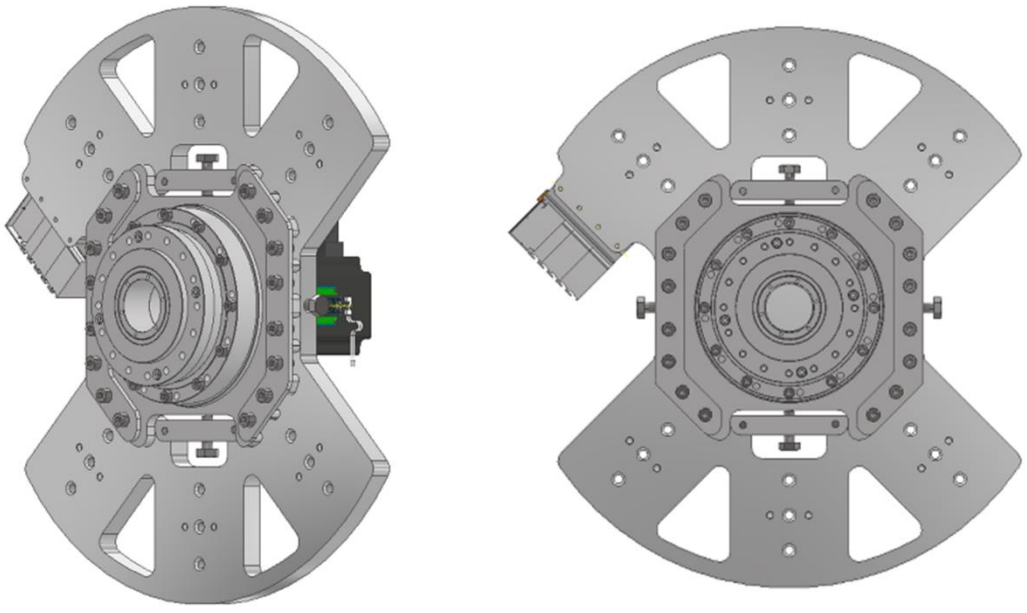

Fig. 43: Inner face of the new central hub

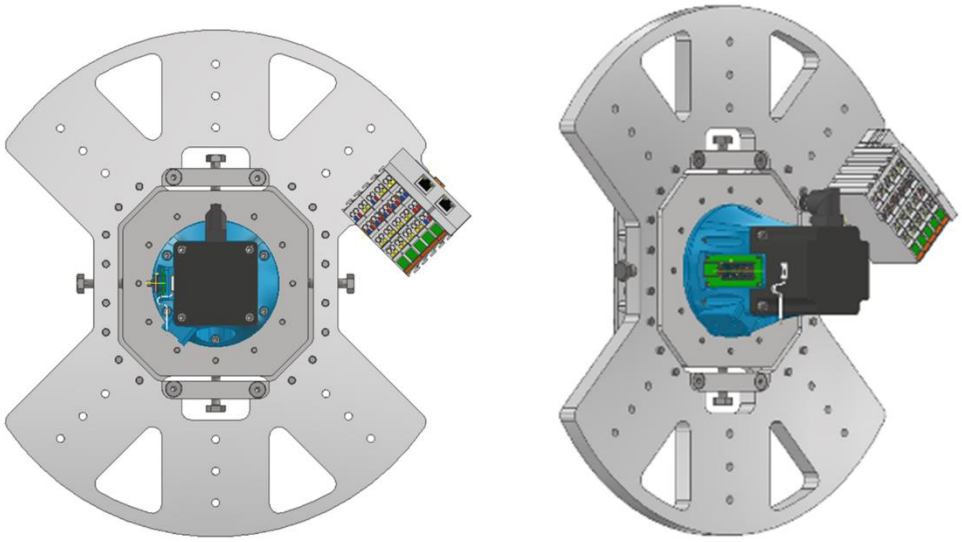

Fig. 44: Outer face of the new central hub

The central piece of the new central hub is held in place by a set of screws and a plate (figure 45) and its position is adjusted by four screws (figure 46).

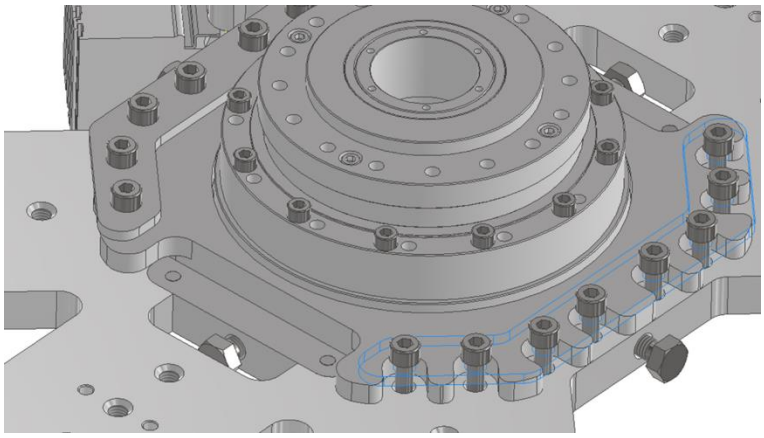

Fig. 45: Stave insertion mechanism

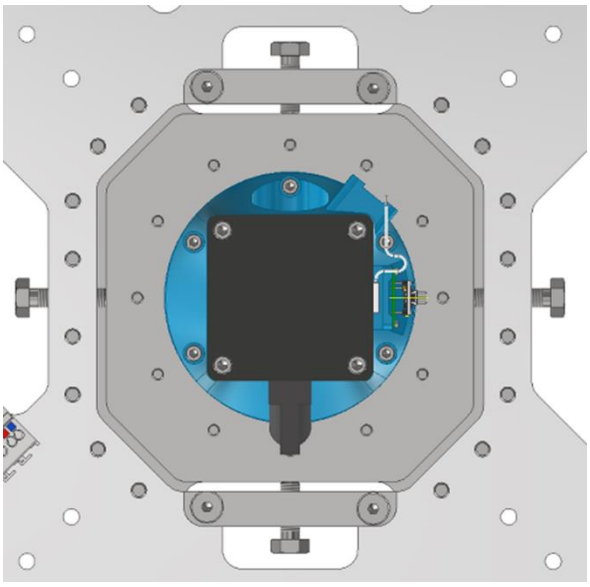

Fig. 46: Stave insertion mechanism

This simplification, however posed a danger of tilting of the center. For this reason, a system of guide rods was developed that would allow alignment in its full range, but would not allow rotation in either plane.

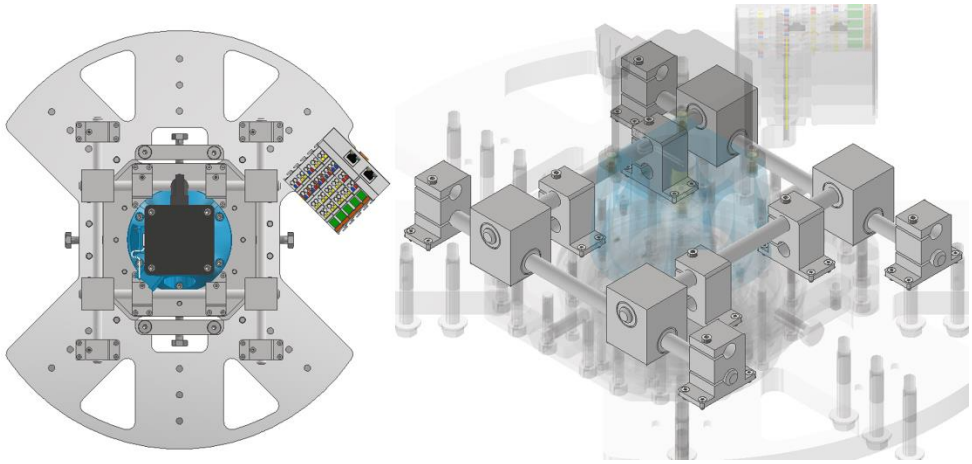

Fig. 47: Mechanism preventing the tilting of the middle piece

5.2 Changes to the carriage

A major change was done to the Z indexing motor, which was moved to the opposite side of the beam to provide more space at the outer end of the beam in order to free up some space for the future installation of the connectors. . This affected the shape of the motor mounting element for the insertion module as it could no longer be placed in its original support. Furthermore, this change affected the shape of the ribs themselves (specifically the last rib) as there was no space where the nut providing the Z indexing movement could be installed.

5.3 Ribs changes

Changes will be made to the ribs to increase the stiffness of the carriage as it is the weakest node of the SIT and its resistance to twisting needs to be increased (see issues in Chapter 7.2). The ribs will be reinforced and the size of the bearings used for the rollers will be changed

5.4 Transition of the control to an industry standard

The change in SIT control required a new cable routing and therefore a new design of cable carriers and their positioning. Furthermore, this modification required a change of all electronics carriers. These changes did not affect the design of the manipulator from the mechanical point of view.

The original idea of using the arduino system was very beneficial from the economical perspective, however, the use of this system proved to be unreliable at this scale.

6 Dimensional analysis

Dimensional analysis was performed to determine the far most positions for positioning the central hubs in relation to each other and the possibility of achieving their alignment.

For non-toleranced parts, the mK tolerance was used for the calculation (Figure 48).

class	up to 0.5	0.5 to 3	over 3 to 6	over 6 to 30	over 30 to 120	over 120 to 400
f (fine)	see below	±0.05	±0.05	±0.10	±0.15	±0.2
m (medium)		±0.10	±0.10	±0.20	±0.30	±0.5
c (rough)		±0.20	±0.30	±0.50	±0.80	±1.2
v (very rough)		-	±0.50	±1.00	± 1.50	± 2.5

Fig. 48: Used tolerances [ISO 2768]

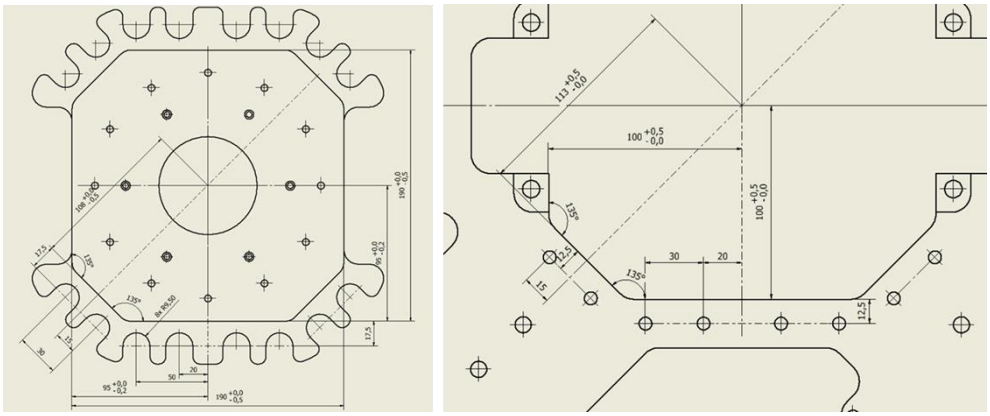

Fig. 49: Partial drawings of the parts of the central hub

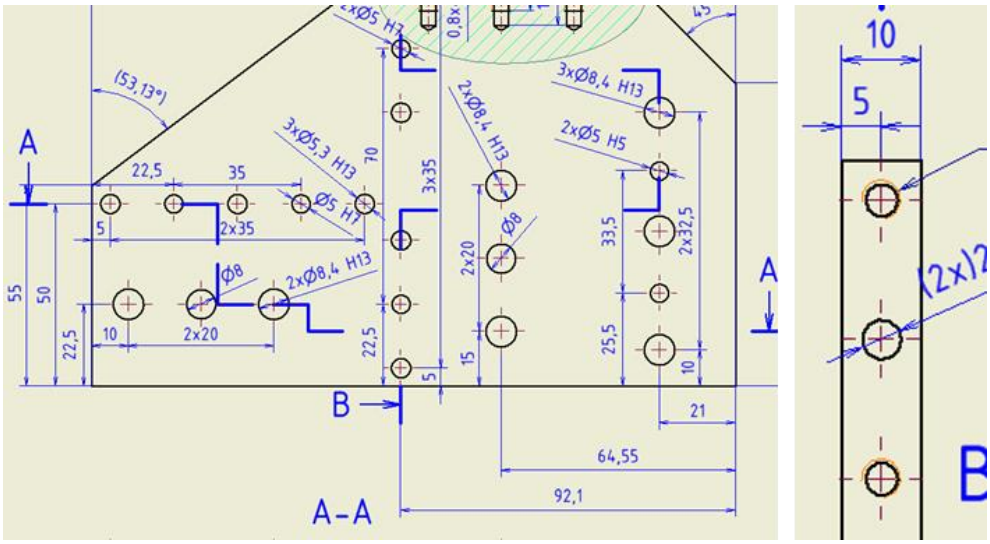

Fig. 50: Partial drawings of the parts of the beam anchor node

The length of the vertical beam is 846 mm and the precision defined by the manufacturer is ±0.2 mm.

Calculation of the far most edge of the beam relative to the axis

The edge of the outer cylinder is considered a rigid point and therefore the dimensional analysis will be calculated in relation to it.

The bracket (part of the beam anchor node) is fixed to the outer cylinder using M8x1.25 bolts into 9 mm hole, which is a clearance of 1 mm or ±0.5 mm. The holes inside the bracket are 21 mm from its edge, meaning the precision is ±0,2 mm. The bracket is connected to the hexagonal plate, where the holes are also 21 mm from the edge, which adds another ±0,2 mm. We do not have to take the fitting of the bolts in consideration, because the alignment pins were utilized.

The plate which creates the base for the beam is positioned at 92.1 mm from the edge, which adds ±0,3 mm. The hole in the plate is positioned 5 mm from the edge, adding ±0,1 mm.

$$L = X + \sum tolerances \quad (4)$$

$$L = X \pm 0{,}5 \pm 0{,}2 \pm 0{,}2 \pm 0{,}3 \ \pm 0{,}1 \quad (5)$$

$$L_{low} = X - 1{,}3 \text{ mm} \quad (6)$$

$$L_{high} = X + 1{,}3 \text{ mm} \quad (7)$$

This means the position of edge of the vertical beam is set with ±1,3 mm precision, where X is the theoretical distance from the outer cylinder anchor point.

Calculation axis of the central hub adjustment possibilities

The edge of the inner piece of the central hub assembly is 95 mm from the axis, with a precision of $^{+0}_{-0{,}2}$ mm. The outer piece of the central hub is 100 mm away from the axis, adding $^{+0{,}5}_{-0}$ mm.

$$S = 100^{+0{,}5}_{-0} - 95^{+0}_{-0{,}2} \quad (8)$$

$$S_{low} = 100 - 95 \quad (9)$$

$$S_{high} = 100{,}5 - 94{,}8 \quad (10)$$

$$S = 5\ mm \quad (11)$$

$$S_{high} = 5{,}7\ mm \quad (12)$$

The axis can have clearance ranging from 5 mm up to 5,7 mm on each side.

Calculation of the inner most edge of the beam relative to the axis

The distance of the hole for the bolt is160 mm from the axis, adding $\pm 0{,}5$ mm. The beam is angored using M8 bolts, adding 1 mm clearance, meaning the dimension is adding $\pm 0{,}5$ mm.

$$N = X \sum tolerances \quad (13)$$

$$N = X \pm 0{,}5 \pm 0{,}5 \quad (14)$$

$$N_{low} = X - 1 \text{ mm} \quad (15)$$

$$N_{high} = X + 1 \text{ mm} \quad (16)$$

Calculation of the position of the axis relative to the outer cylinder

The position of the axis, relative to its theoretical position is equal to the sum of the tolerances.

$$F' = N + L \pm 0{,}2 + \sum X \quad (17)$$

$$F = N + L \pm 0{,}2 \quad (18)$$

$$F_{low} = N_{low} + L_{low} - 0{,}2 \quad (19)$$

$$F_{low} = -1 - 1{,}3 - 0{,}2 \quad (20)$$

$$F_{high} = N_{high} + L_{high} + 0{,}2 \quad (21)$$

$$F_{high} = 1 + 1{,}3 + 0{,}2 \quad (22)$$

$$N_{low} = -2{,}5 \text{ mm} \quad (23)$$

$$N_{high} = +2{,}5 \text{ mm} \quad (24)$$

Evaluation of the calculations

In the worst scenario, the axis of the central hubs will be 2,5 mm off from the theoretical position, meaning the total of 5 mm will be needed for the adjustment. The current systém offers 10 mm adjustment in the worst scenario and 11,4 in the best, meaning the central hubs can be always aligned.

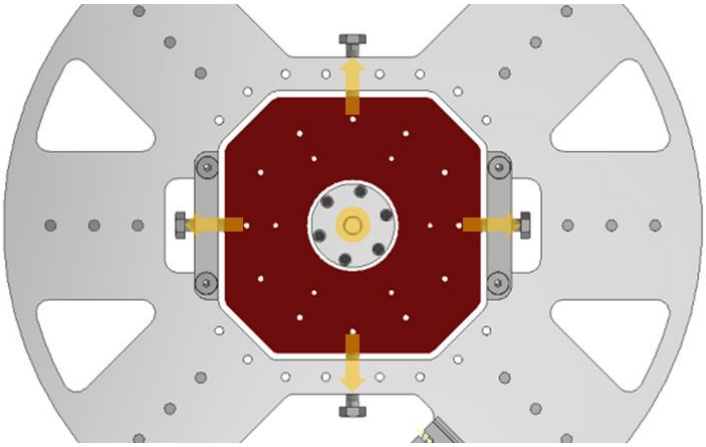

Fig. 51: Adjustment directions and the required circular field for the central hub axis

7 Deformation analysis

7.1 Outer frame deformation analysis

The analysis of the external structure was conducted with a total load of 800 N and a torque of 450 Nm.

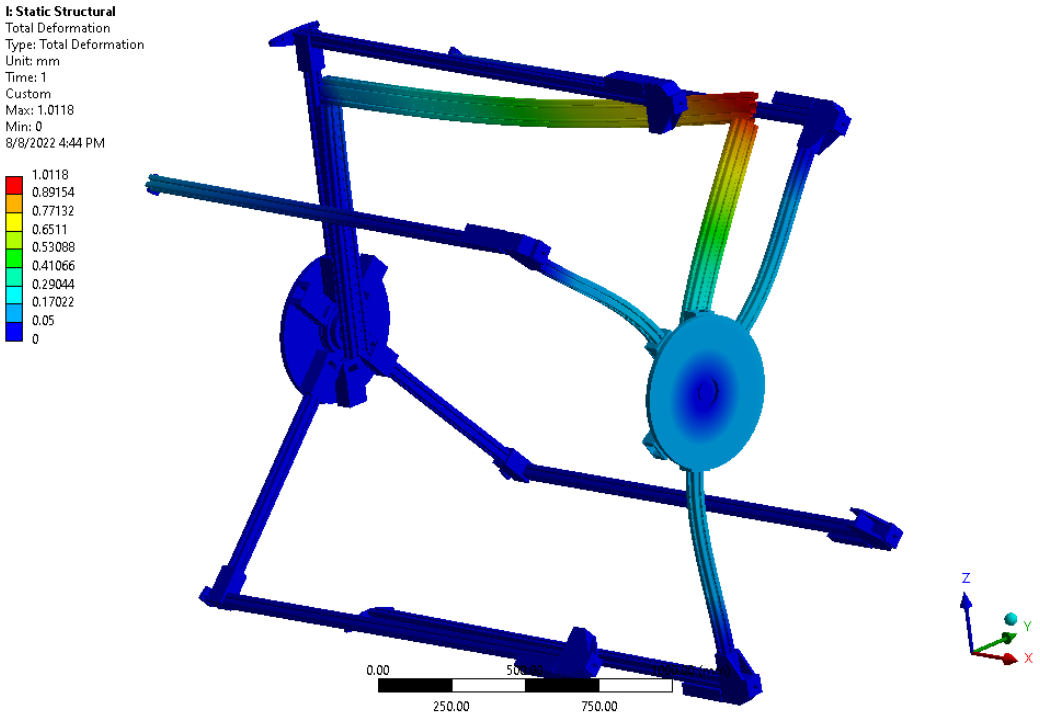

Fig. 52: Deformation of the outer frame caused by applying 400 N on the beam (Y axis direction)

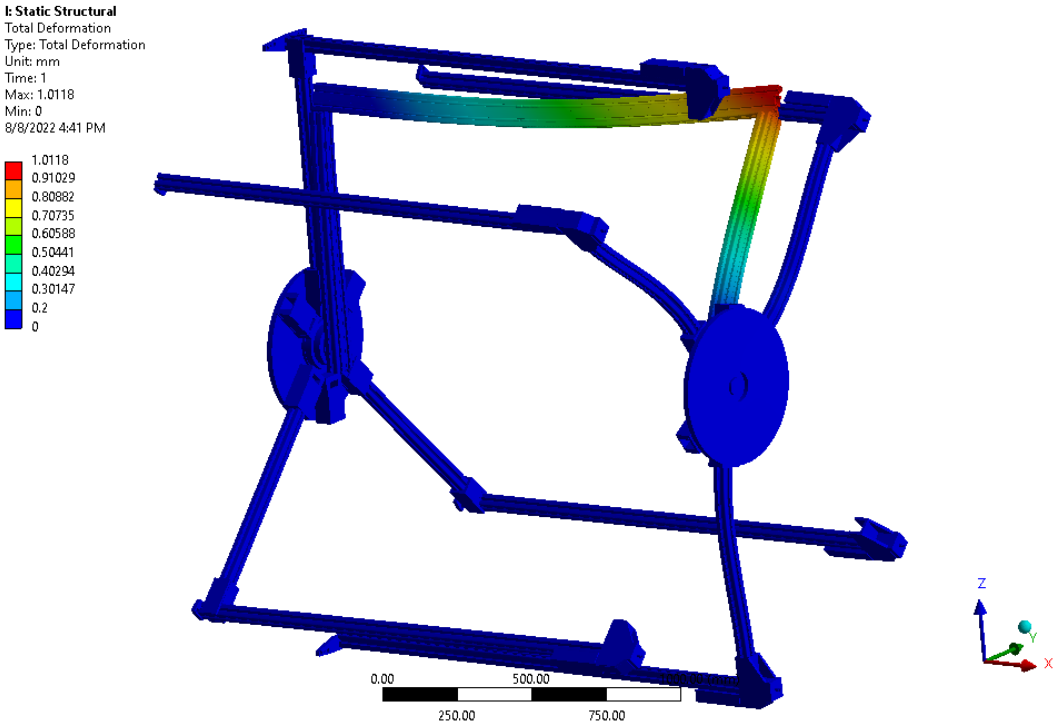

Fig. 53: Deformation of the outer frame caused by applying 400 N on the beam (Y axis direction), colour scale shows deformations above 0,2 mm

The analysis of the outer frame deformations revealed that the forces cause the frame to deform by less than 0.2 mm, if only 3 legs are used on each side, The analysis also shows that the outer central hub is more susceptible to deformations, which is caused by the offset design of the structure. The results are in agreement with the expectations. The stiffness of the outer frame seems to be very high, however, the simulation shows that, the beams placement, relative to the force, has a major impact on the deformations. For this reason, it is adviced to use as many of the beams as possible.

7.2 Arm assembly deformation analysis

Arm assembly (carriage with the horizontal beam) deformation analysis was performe d for the force applied by the operator during manipulation of the stave with the box. First, the direction of force application in which the greatest deformation occurs was determined. The YZ plane was chosen as the force application plane and then the arm was loaded with 15 N, 50 N and 100 N. Subsequently, the analysis was performed for the force loading from the stave and the box only. The results are sumarised in the tables 1 and 2.

Assembly loaded by force from the operator (without the stave in the box)

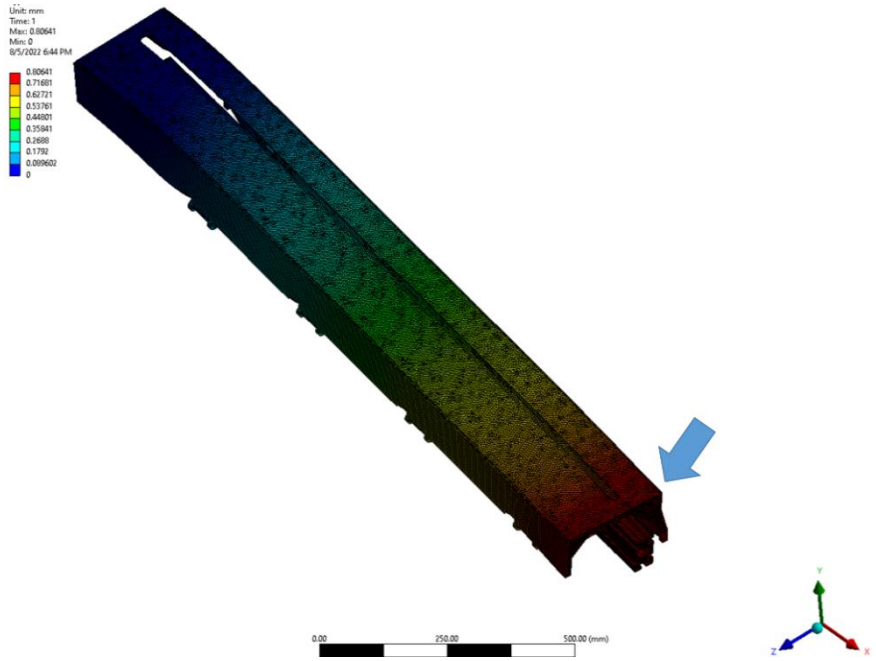

Fig. 54: Carriage loaded with a force of 15 N

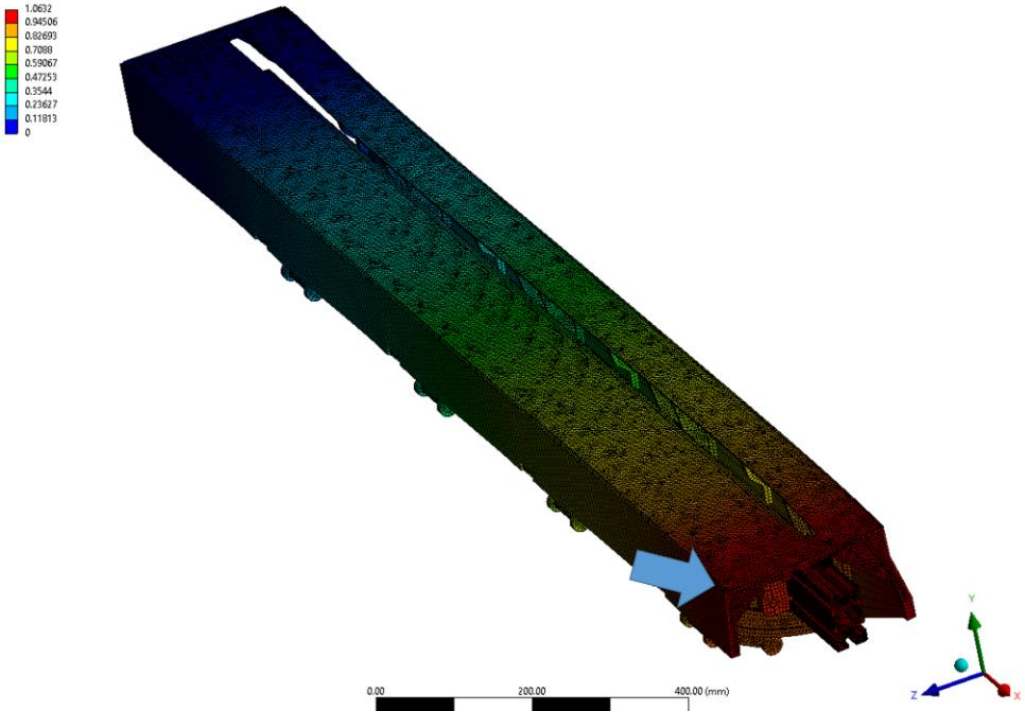

Fig. 55: Carriage loaded with a force of 15 N

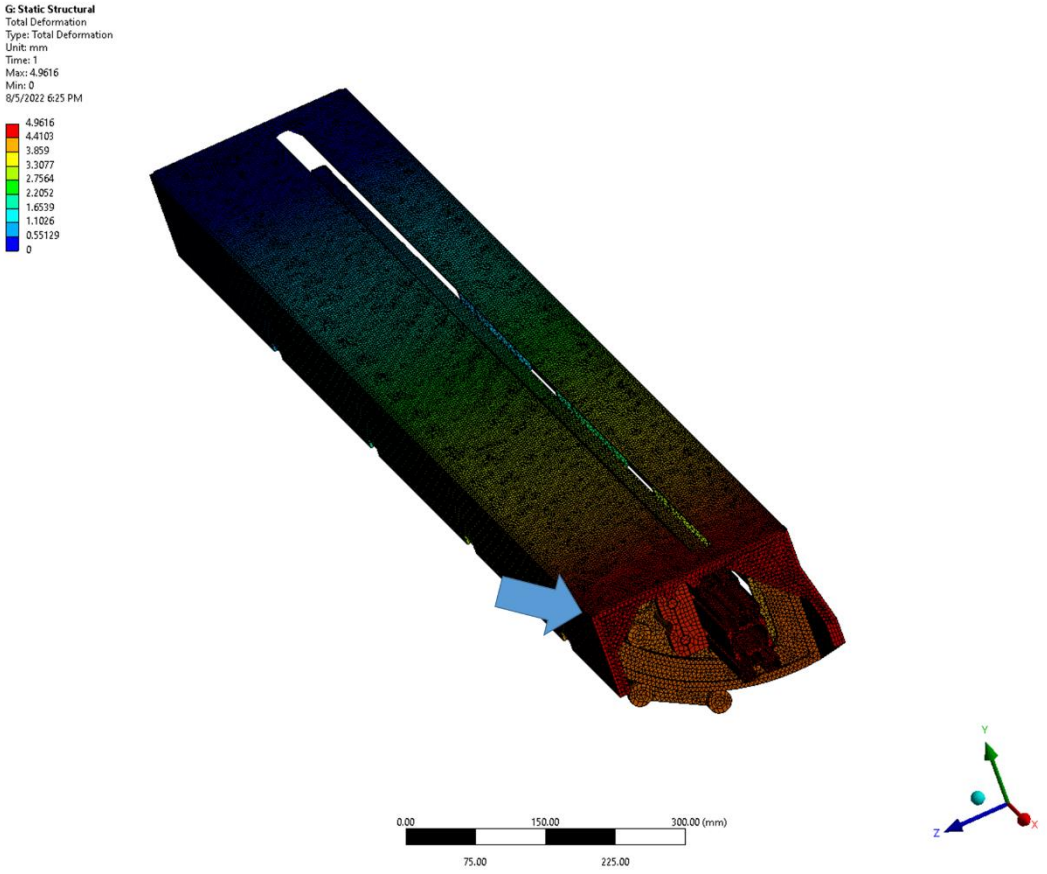

Fig. 56: Carriage loaded with a force of 50 N

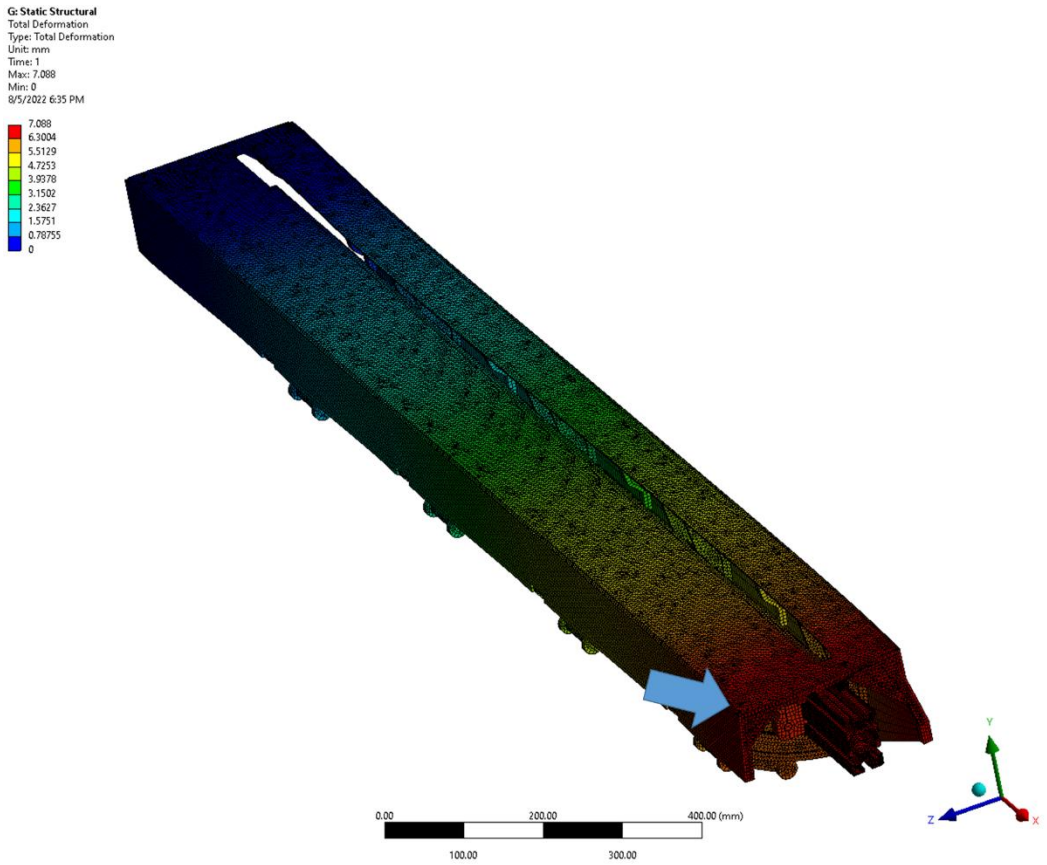

Fig. 57: Carriage loaded with a force of 100 N

Force	max deformation from the force (+Z; -Y) [mm]	max deformation from the force (-Z; -Y) [mm]
15 N	0.8060	1.0630
50 N	N/A	4.9620
100 N	N/A	7.0880

Tab. 1: Comparison of the deformations for different directions and forces

The table 1 shows that the difference in deformation depends on the direction from which the force was applied. In this case, the maximum deformation was for the Z=-; Y=- direction, so all the subsequent deformations (for 50 N and for 100N) were calculated for this direction. Although the construction is fairly stiff for the application of the forces from just the stave and the box, its stiffness in torque (mainly the stiffness of the shell enveloping the carriage) needs to be improved. Possible solution for this issue could be fully enveloping the carriage instead of having the shell split in two as it is in present.

Assembly loaded by force from the stave and the box only

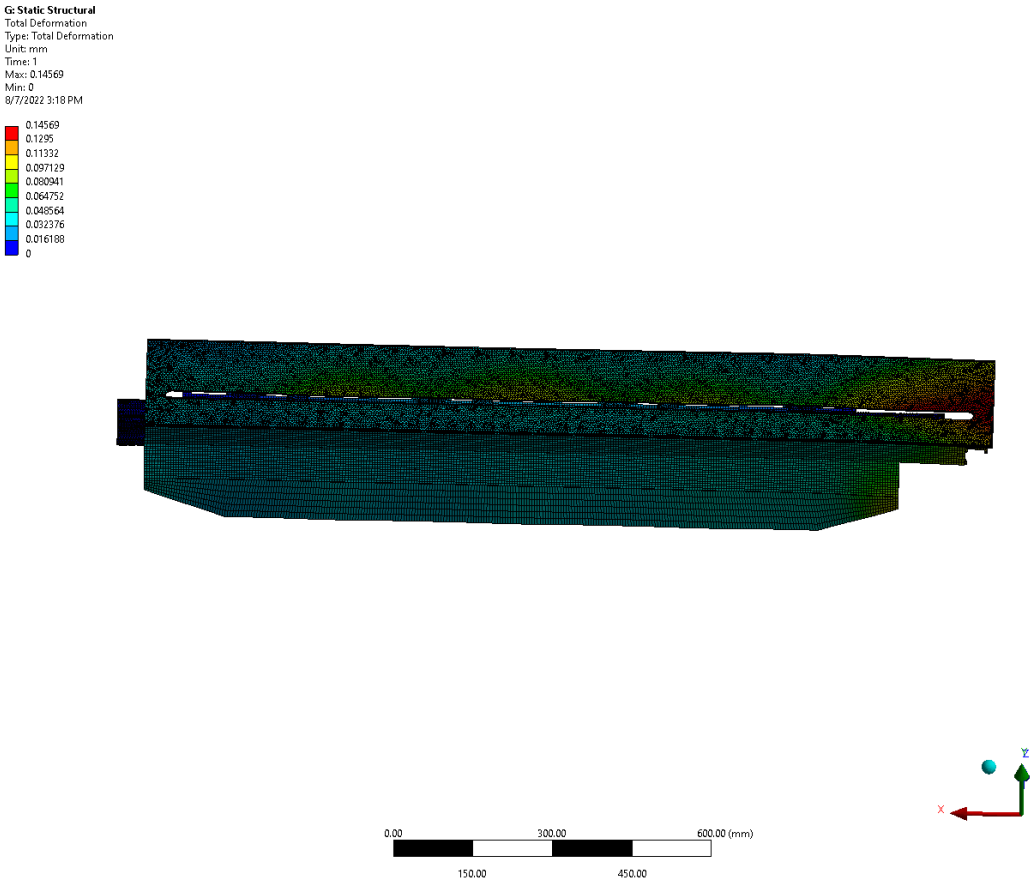

Fig. 58: Carriage loaded with a force of 150 N in the Y axis (solid ribs)

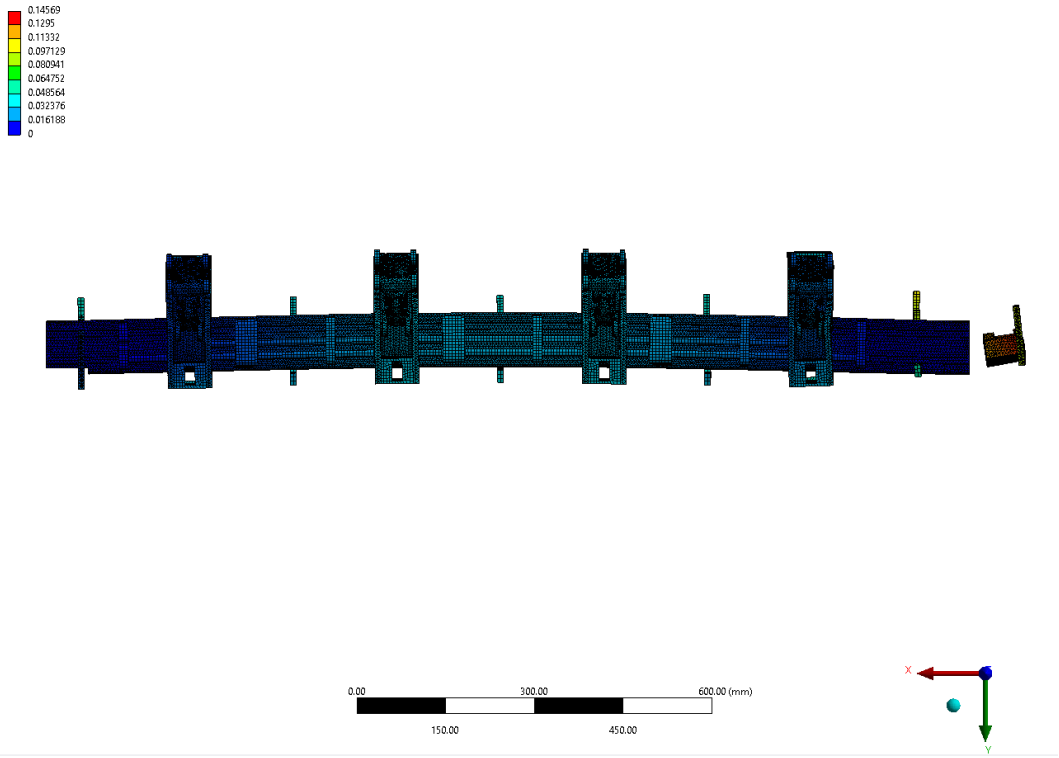

Fig. 59: Carriage loaded with a force of 150 N in the Y axis – horizontal beam detail (solid ribs)

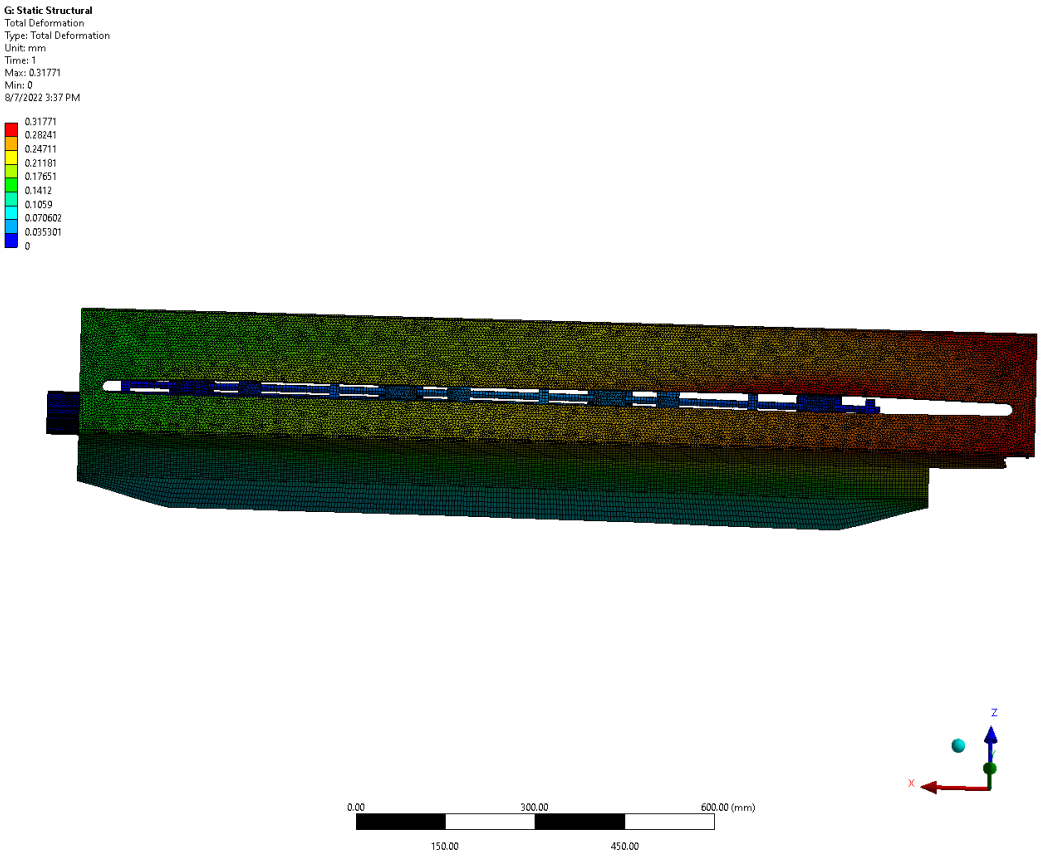

Fig. 60: Carriage loaded with a force of 150 N in the Z axis (solid ribs)

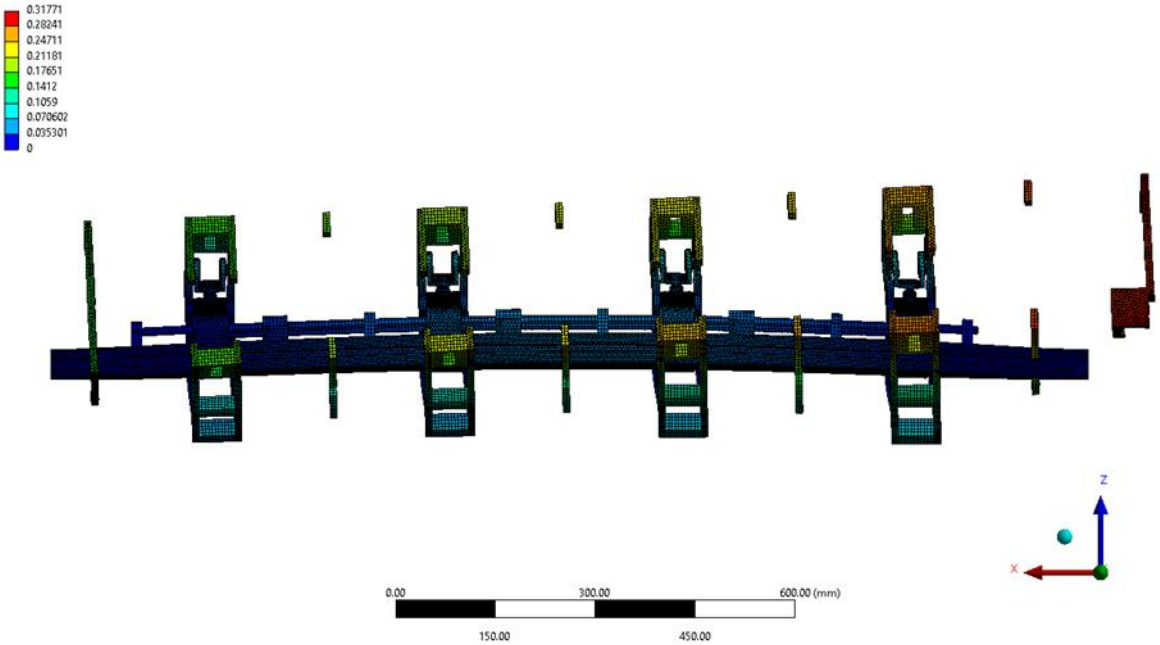

Fig. 61: Carriage loaded with a force of 150 N in the Z axis– horizontal beam detail (solid ribs)

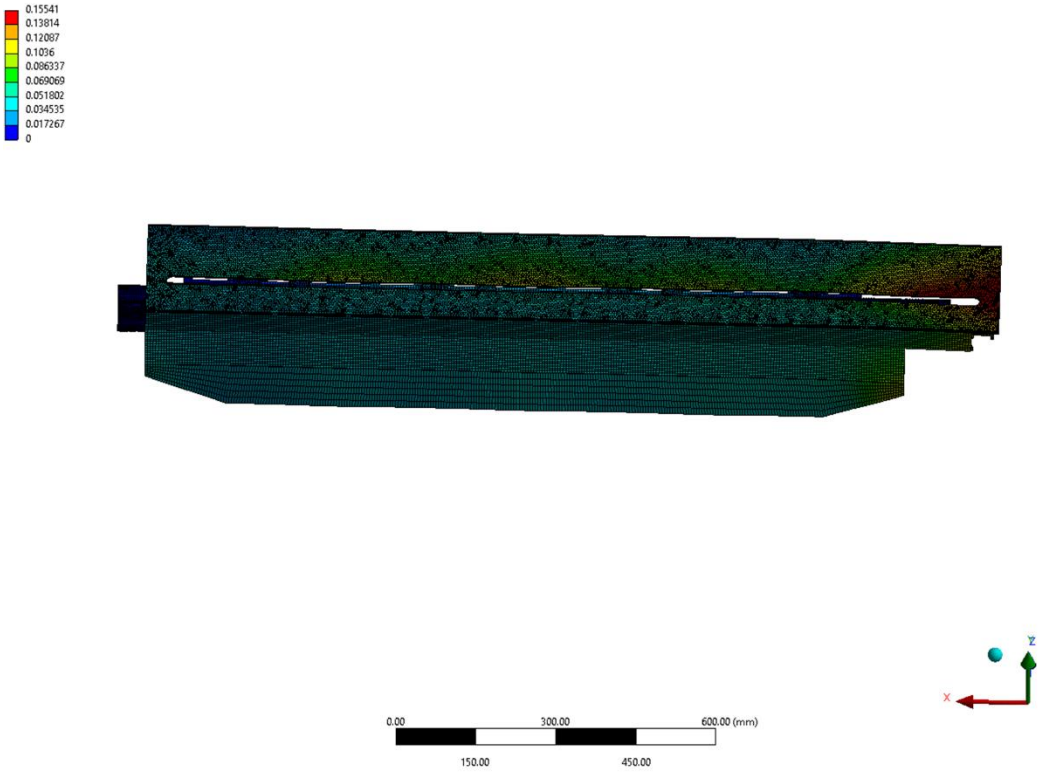

Fig. 62: Carriage loaded with a force of 150 N in the Y axis (ribs with matrix)

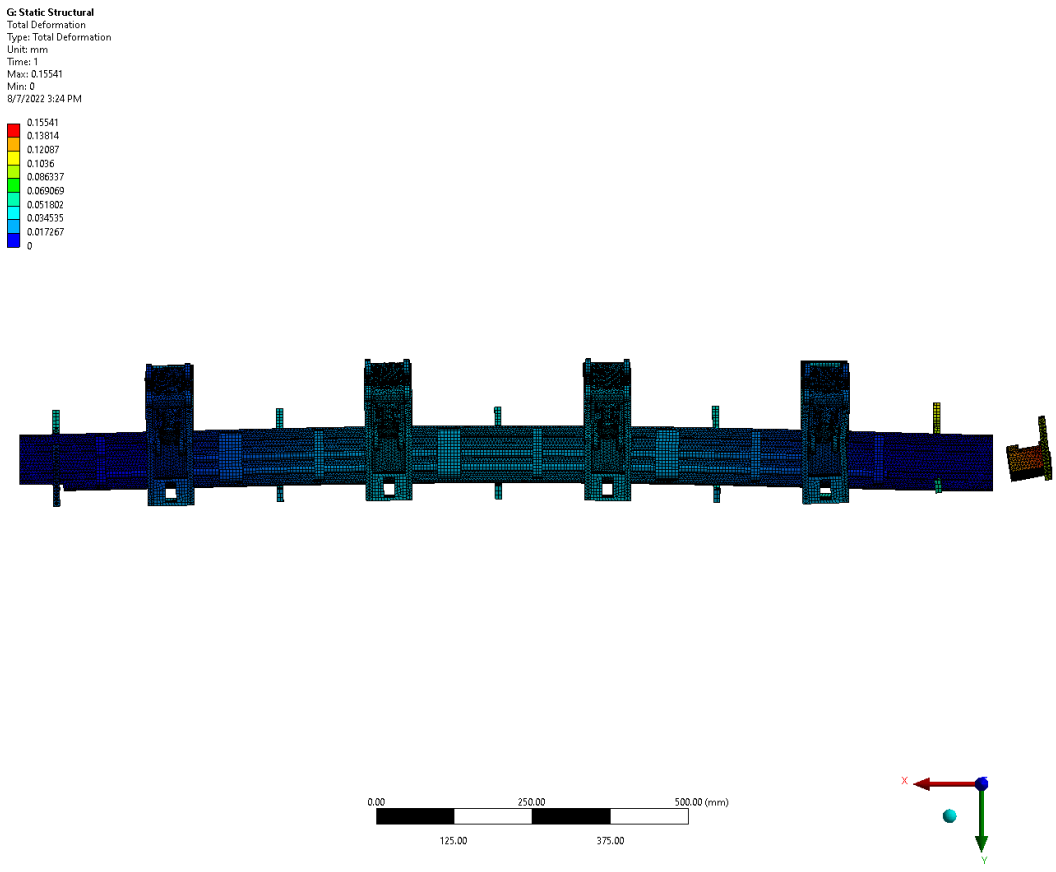

Fig. 63: Carriage loaded with a force of 150 N in the Y axis – horizontal beam detail (ribs with matrix)

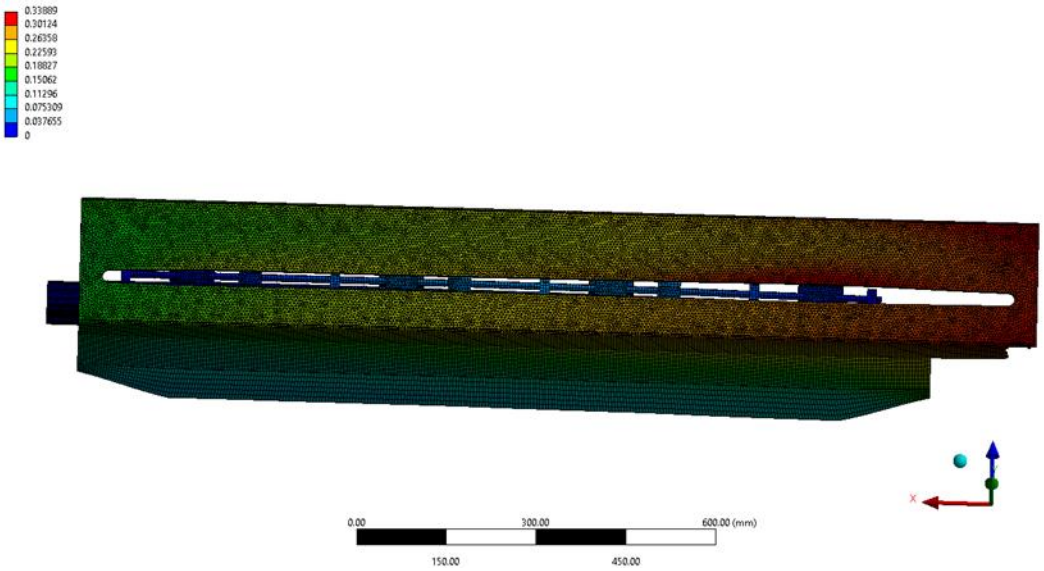

Fig. 64: Carriage loaded with a force of 150 N in the Z axis (ribs with matrix)

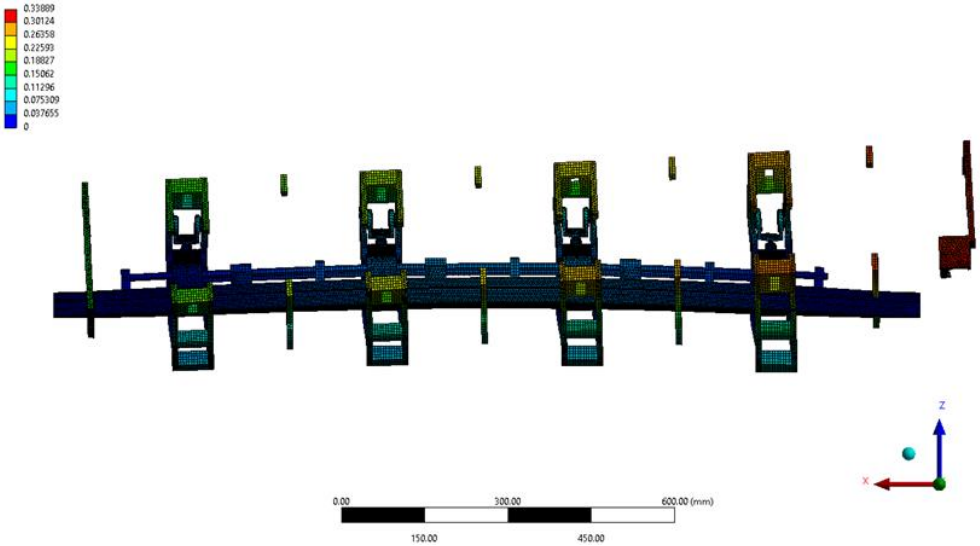

Fig. 65: Carriage loaded with a force of 150 N in the Z axis– horizontal beam detail (ribs with matrix)

	max deformation from the axis force [mm]		Beam deformation from the axis force [mm]	
	Axis Y	**Axis Z**	**Axis Y**	**Axis Z**
Rib with matrix	0.155	0.339	0.051	0.110
Full rib	0.146	0.318	0.047	0.104

Tab. 2: Comparison of the deformations for different models

The analysis confirmed the stiffness of the assembly. As the table 3 indicates that, the maximum deformation occurs when the SIT is in the 3:00 or 6:00 positions.

The most vulnerable part of the carriage is its shell. The maximum measured deformation of the beam was 0.110 mm for the matrix model and 0.104 for the solid model.

It is also apparent from the table that, the matrix has only minor impact on the simulation.

7.3 Stiffness analysis of the ribs for different designs

For the deformation analysis, the model consisting of plains was created in order to simulate the 3D printed part. Each plane had then their properities assigned by a script. The properities were taken from the slicer settings (figure 66).

A total of three designs were analysed and loaded in four main directions and their deformations were investigated. The loading directions are indicated by the arrow. The loading force was 20 N, i.e. close to 1/8 of the weight of stave with the box. The results are summarised in table 3.

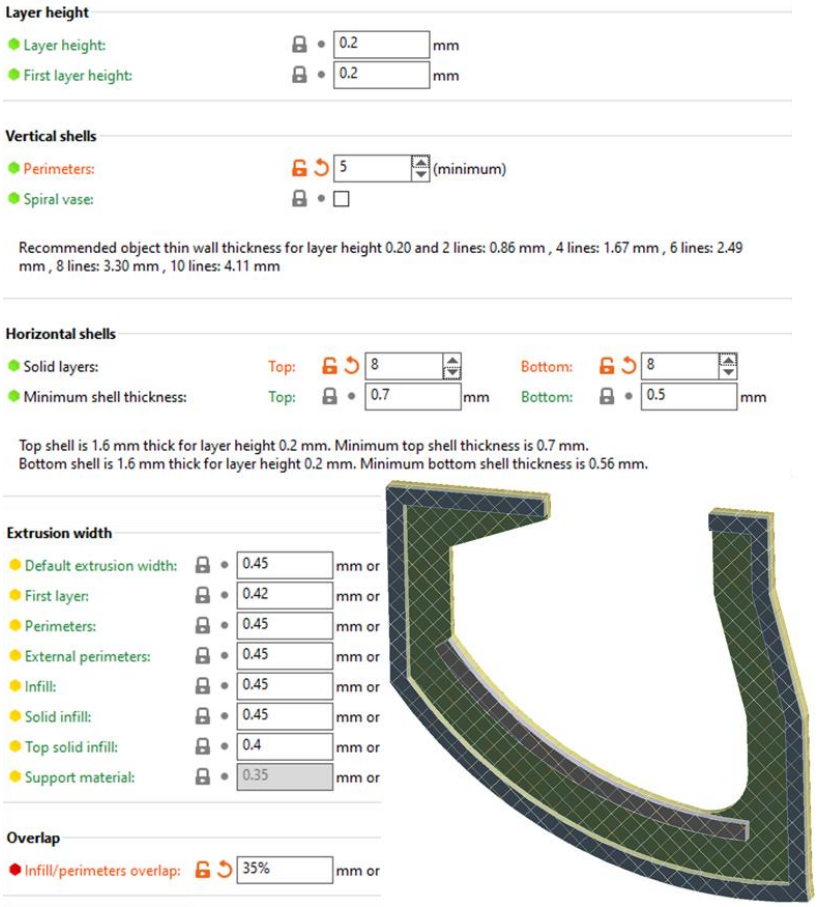

Fig. 66: Input data for the rib analysis

Currently used ribs (PLA)

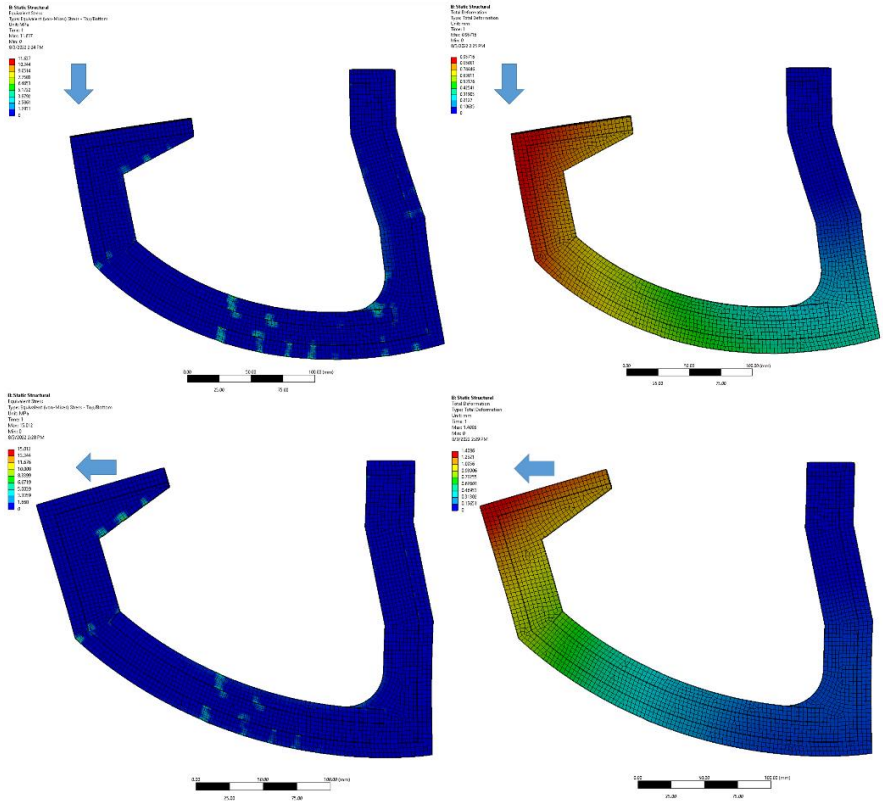

Fig. 67: currently used rib with the matrix deformation and stress analysis

Stiff ribs (PLA)

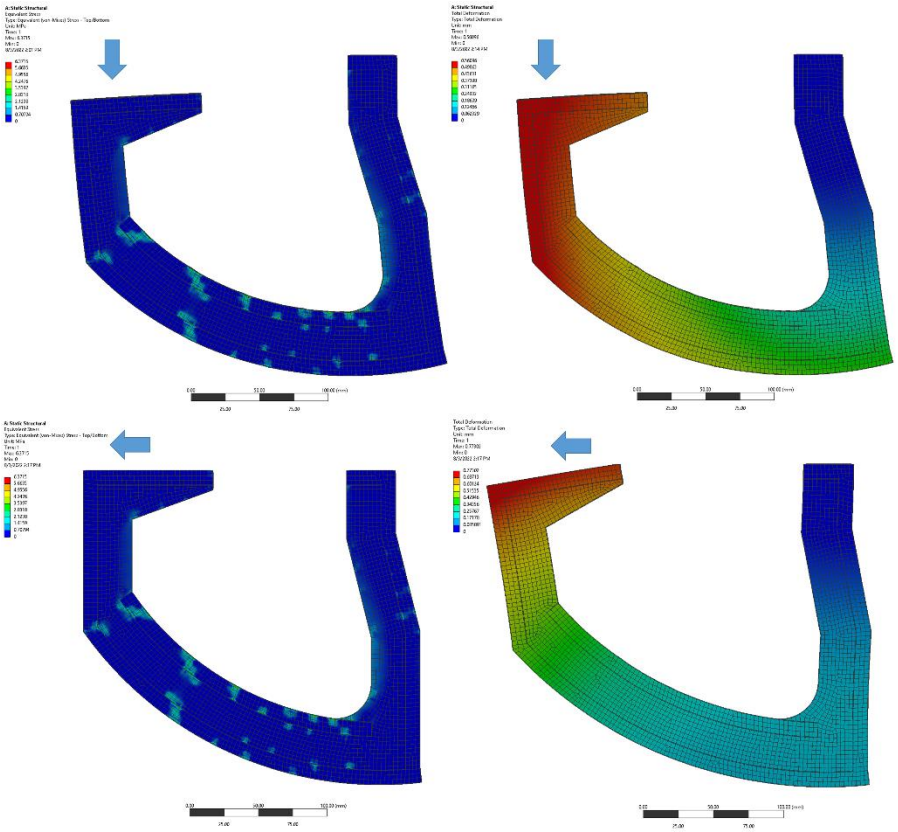

Fig. 68: Stiff rib with the matrix deformation and stress analysis

Aluminum ribs

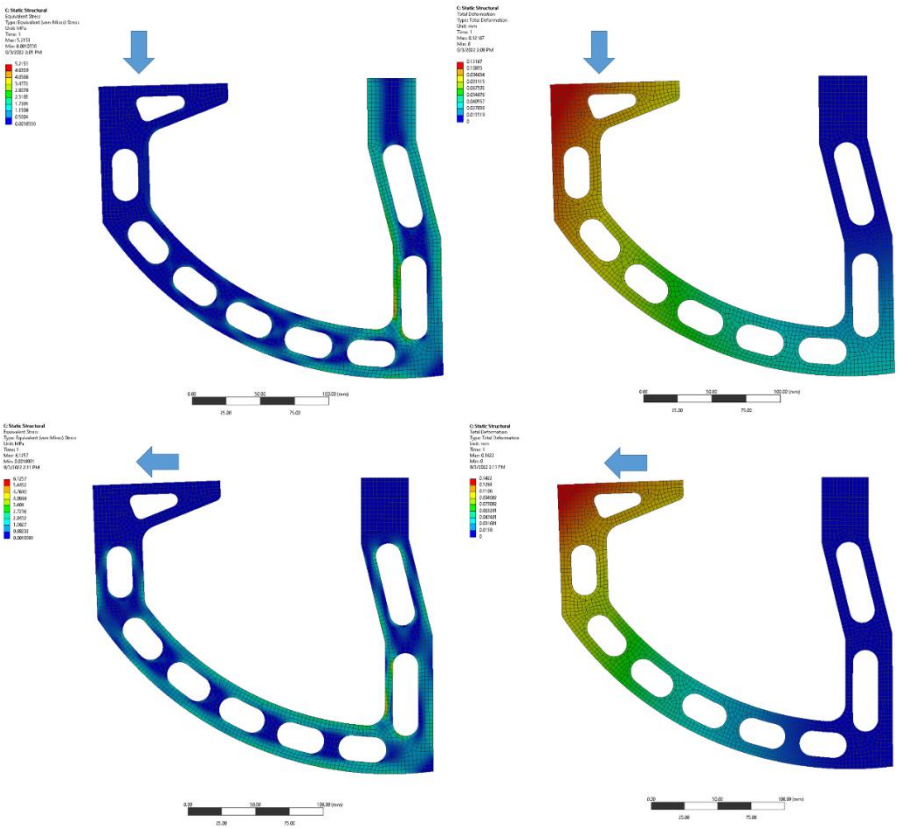

Fig. 69: Aluminum rib deformation and stress analysis

Currently used ribs without the matrix (solid model, PLA)

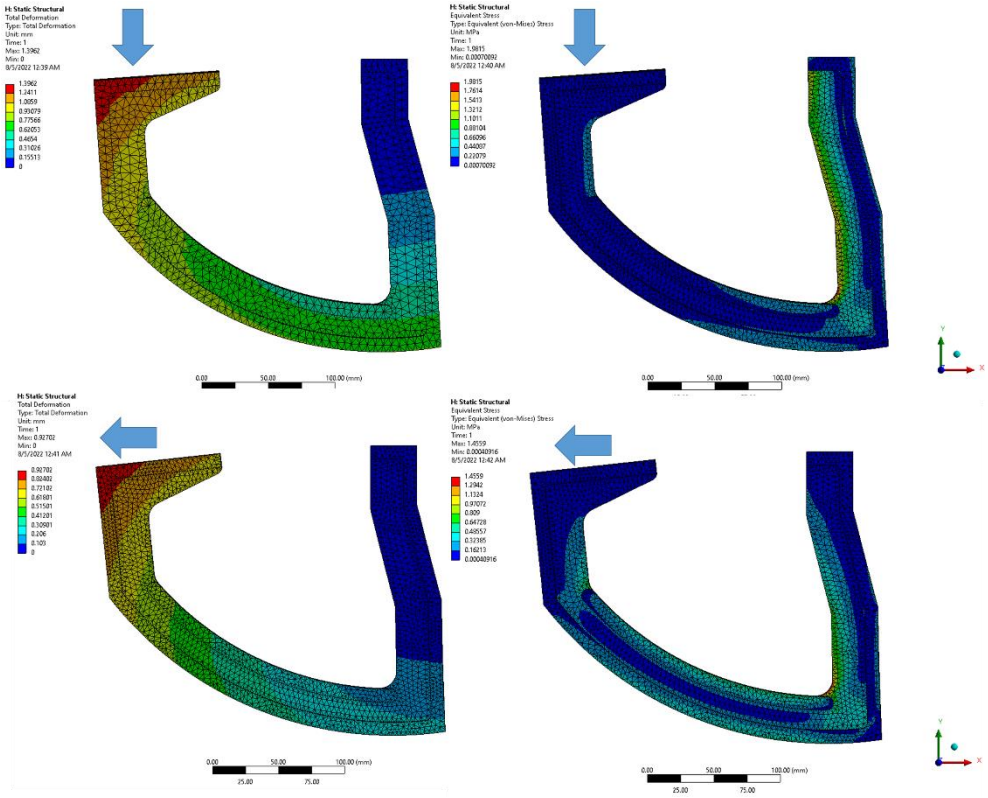

Fig. 70: Solid rib (PLA) deformation and stress analysis

	Deformation from the axis force [mm]	
	Axis X	**Axis Y**
Currently used ribs (PLA)	0,957	1,406
Stiff ribs (PLA)	0,773	0,561
Aluminum ribs	0,122	0,142
Currently used ribs without the matrix (solid model, PLA)	0,927	1,396

Tab. 3: Comparison of the deformations for different models

The table 3 shows that the difference in deformation for the analysis with and without the matrix being modeled is negligible. It can also be seen that the stiffening of the lower part of the rib resulted in a reduction in deformation of tens of percent in exchange for a 50 g increase in weight. The use of an aluminum rib reduced the deformation by up to 90%, however, there would be an increase in the weight of the arm of 521 g.

8 Conclusion

The SIT was designed according to the requirements set by the contractor, drawings were created and the machined parts were manufactured according to the production drawings (attachments 4-7). In addition, all printed parts were printed at CTU and the first iteration of the equipment was already built and tested in the CTU laboratories in Prague and subsequently packed and shipped to the RAL laboratories in Oxford (attachment 1), where the tooling was tested.

The deformation analysis was performed on the ribs in order to optimise their design. The analysis shows that, the stiff rib design offers a huge increase of stiffness in exchange for increasing the weight of the whole assembly by only 50 g. The aluminum ribs offer a even stiffer solution. Their deformation was up to 90% smaller, compared to the currently used design, but their use would mean adding a relatively large mass to the assembly.

Another reason for this analysis was to determine the impact of the presence of the matrix in the model. This factor appears to have insignificant impact on the of the FE analysis results, so except for the analysis of the carriage (arm assembly) the solid rib model was used.

The arm assembly design analysys was a very important step. The design team was aware of its vulnerability to the outer forces, but the analysis helped us to determine what the problematic nodes might be. As is aparent from the analysis, this part of the SIT has a tendency to twist when a external force is applied, which represents an issue and a potentional danger to its integrity since it is very vunerable to torque and easily deforms when exposed to it.

The external forces (from the operator) were not taken into consideration during development of the first iteration. It only took into the consideration the forces from the device itself and the weight of the box with the stave. This finding was subsequently confirmed by RAL. The design team is currently focused on solving this issue, but no solution was fully developed yet.

The deformation analysys confirmed that, the SIT is fully operational with only half vertical beams installed. The deformation of the structure itself is <0,3 mm after loading the stave

The software team is currently engaged in the development and testing of the software for the optical alignment and control of the SIT using it. Based on the testing, the design team is working on a second iteration of the device to address the flaws of the first iteration. Some of these modifications have already been introduced within this thesis, but not all have been developed yet. The continuation

of this project includes the finalization of the arm assembly (carriage and the horizontal beam) and its presentation in autumn. Subsequently, the completion of the entire SIT V2.0 assembly and its testing and presentation.

The final stage of this project will be the insertion of all the staves into the ITk outer cylinder.

LIST OF REFERENCES USED

[1] H. Pernegger, The Pixel Detector of the ATLAS Experiment for LHC Run-2, CERN Physics department, 2015 https://cds.cern.ch/record/1985432/files/ATL-INDET-PROC-2015-001.pdf

[2] CERN. Geneva. The LHC experiments Committee, Technical Design Report for the ATLAS Inner Tracker Pixel Detector, ATLAS Collaboration 2017

[3] Sven Wonsak, The ATLAS ITk Strip Detector System for the Phase-II LHC Upgrade, ATLAS Collaboration 2019

[4] “Technical design report for FDR Strip stave insertion tooling and procedure”, 23.09.2021

[5] Catalogue teatechnic.cz [online] [quoted 07.08.2022] https://www.teatechnik.cz/typ-vts/

[6] AUTHOR UNNAMED igus.com [online] [quoted 07.08.2022] https://www.linquip.com/blog/worm-gearbox-working-principle/

[7] JAN BRUS, DESKRIPCE RŮZNÝCH DRUHŮ PŘEVODOVEK HARMONIC-DRIVE, VUT V BRNĚ FS ÚSTAV AUTOMOBILNÍHO A DOPRAVNÍHO INŽENÝRSTVÍ 2008

[8] AUTHOR UNNAMED igus.com [online] [quoted 02.08.2022] https://www.engineeringclicks.com/harmonic-drive/

[9] ZTS ZÁVODY ŤAŽKÉHO STROJÁRSTVA. Harmonické prevodovky. ZTS Závody ťažkého strojárstva, 1990.

[10] Catalogue boschrexroth.com [online] [quoted 04.08.2022] https://www.boschrexroth.com/en/xc/products/product-groups/assembly-technology/basic-mechanic-elements/strut-profiles

[11] Catalogue boschrexroth.com [online] [quoted 04.08.2022] https://www.boschrexroth.com/en/xc/products/product-groups/assembly-technology/basic-mechanic-elements

[12] Catalogue lin-tech.hennlich.cz [online] [quoted 07.08.2022] https://lin-tech.hennlich.cz/produkty/linearni-vedeni-a-kulickove-srouby-linearni-vedeni-valive-linearni-vedeni-s-kulickovym-retezem-636.html

[13] Catalogue lin-tech.hennlich.cz [online] [quoted 07.08.2022] https://lin-tech.hennlich.cz/produkty/linearni-vedeni-a-kulickove-srouby-linearni-vedeni-valive-miniaturni-vedeni-649.html

[14] Catalogue teatechnic.cz [online] [quoted 04.05.2022] https://www.teatechnik.cz/obehovymi-kulickami/

[15] Catalogue hiwin.fr [online] [quoted 07.08.2022] https://hiwin.fr/fr/Produits/Guidages-sur-rail-profil%C3%A9/c/4354

[16] Catalogue igus.com [online] [quoted 03.08.2022] https://www.igus.ch/drylin/linear-guide

[17] Catalogue Igus.com [online] [quoted 07.08.2022] https://www.igus.ch/iglidur/gleitlager

[18] AUTHOR UNNAMED igus.com [online] [quoted 07.07.2022] https://blog.drupa.com/wp-content/uploads/2014/11/overview.png?fbclid=IwAR0riQ7jrg_jPXpHK0HsuGHFD04No2EcnwHII57xUk2DtUgbXa1FP-3feF8

[19] AUTHOR UNNAMED ge.com [online] [quoted 01.08.2022] https://www.ge.com/additive/additive-manufacturing?utm_source=google&utm_medium=paid_advertising&utm_campaign={campaign}&utm_term=additive%20manufacturing%20technologies&utm_content=manufacturing&gclid=Cj0KCQjwxb2XBhDBARIsAOjDZ37-FhVHQXmjkKjHL38AbDWVXMmGzK8A47RLx7QwlLdFWsohGePNiCQaAgZrEALw_wcB

[20] Ondřej Stříteský, Josef Průša, Martin Bach, Základy 3D tisku s Josefem Průšou Prusa Research a.s. 2019

[21] https://www.filament-pm.cz/?gclid=Cj0KCQjwxb2XBhDBARIsAOjDZ35h5gzLViJrrgAmf1MyhWvsz0iZOpzCXvtxNSDnhkuF4pT10-pWkbUaAu5TEALw_wcB

[22] AUTHOR UNNAMED all3dp.com [online] [quoted 02.07.2022] https://all3dp.com/1/3d-printing-materials-guide-3d-printer-material/

[23] Jiří Leinveber, Pavel Vávra, Strojnické tabulky páté vydání, Albra 2011

[24] AUTHOR UNNAMED qfinsoft.co [online] [quoted 04.08.2022] https://www.qfinsoft.co.za/blog/ansys-mechanical-scripting

[25] Martin Janda, AT2-IC-EP-0001 v.2.0 ITk Envelope Drawing 2021

[26] AUTHOR UNNAMED .engineeringclicks.com [online] [quoted 06.08.2022] https://www.engineeringclicks.com/harmonic-drive/

[27] AUTHOR UNNAMED linquip.com [online] [quoted 04.08.2022] https://www.linquip.com/blog/worm-gearbox-working-principle/

LIST OF ABBREVIATIONS

EoS – end of structure (card)

SIT – Stave Insertion Tooling

LHC – Large Hadron Collider

RAL - Rutherford Appleton Laboratory

SL – Stereolithography

PJ – Photopolymer jetting

BBJ – inder jetting

LM – Laser beam melting

EBM – Electron beam melting

FDM – Fused deposition modeling

LS – Laser sintering

MJ – Material jetting

FE – Finite elements

LIST OF ATTACHMENTS

[1] Save Insertion Tooling assembly instructions

[2] Drawing SIT-00-00-00-000

[3] Drawing SIT-05-01-00-001

[4] Drawing SIT-06-00-00-000

[5] Drawing SIT-06-00-00-001

[6] Drawing SIT-06-00-00-003

[7] Drawing SIT-06-00-00-005